1   **On the sources of uncertainty in the sub-3 nm particle concentration measurement**

2   J. Kangasluoma and J. Kontkanen

3   Department of Physics, P.O. Box 64, 00014, University of Helsinki, Helsinki, Finland
4
5   **Abstract**
6
7   The number of experiments characterizing sub-3 nm aerosol particle dynamics has increased
8   significantly over the recent years. In these experiments, it is essential to know/determine size
9   resolved particle number concentrations accurately. Despite particle concentration measurement
10   being relatively simple experiment, it can contain large uncertainties from various sources in the sub-
11   3 nm size range. In this study we aim to identify and examine some of these sources. We simulated
12   four different condensation particle counters (CPCs) (TSI 3777, ADI vWCPC, Airmodus A11 and an ideal
13   CPC with d50 (lowest detection threshold) of 1.5 nm) and one differential mobility analyzer (DMA) (TSI
14   nano DMA) and study the resulting uncertainties when using them to measure three different particle
15   size distributions. First, we show that Poisson uncertainty √N/N represents the statistical uncertainty
16   in all CPC and DMPS counting experiments. Second, the state-of-the-art DMA-CPC particle sizing
17   system is examined with respect to counting statistics. Third, the performance of the instruments is
18   assumed to be well-known, and instrumental non-idealities and the inversion routine are assessed.
19   Fourth, ±0.5 nm offset is inserted to the CPC d50, and its effect on the measured particle concentration
20   is examined. Our results highlight the importance of knowing the CPC d50 accurately to narrow down
21   the particle concentration uncertainty. Furthermore, the results show that the current DMA-CPC
22   measurements are subject to considerable counting uncertainty in low particle concentration
23   environments. Based on the analysis we summarize suggestions for further research and instrumental
24   development for more accurate sub-3 nm particle concentration measurements in the future.
25
26   **1 Introduction**
27
28   In recent years, great efforts have been made to understand the formation and growth of sub-3 nm
29   particles in the atmosphere (Jiang et al., 2011c; Kulmala et al., 2013; Bianchi et al., 2016; Sipilä et al.,
30   2016) and in controlled conditions in chamber studies (Kirkby et al., 2011; Almeida et al., 2013; Ehn et
31   al., 2014; Kirkby et al., 2016). Simultaneously, a need has emerged for the optimization of specific
32   industrial applications and particle synthesis methods related to phase transition of vapor to liquid or
33   solid nanoparticles (Alanen et al., 2015; Kangasluoma et al., 2015; Carbone et al., 2016; Nosko et al.,
34   2016; Wang et al., 2016, 2017). The current view is that atmospheric gas-to-particle conversion occurs
35   via formation of molecular clusters from low-volatile vapors and their subsequent growth to larger
36   aerosol particles (e.g. Kulmala et al., 2014). The growth of the clusters is hindered e.g. by coagulation
37   losses to the aerosol population and diffusional losses to the near-by surfaces, both of which are the
38   highest for the smallest sizes. Therefore, particle populations with a continuous formation of the
39   molecular clusters are typically characterized by a strong decrease in the particle concentration with
40   the increasing particle size in the sub-3 nm size range (Jiang et al., 2011c; Kulmala et al., 2013).
41   A direct measurement of the particle formation includes both chemical characterization of the
42   nucleating species by mass spectrometric methods (Smith et al., 2010; Jokinen et al., 2012; Ehn et al.,
43   2014; Lopez-Hilfiker et al., 2015) and a size resolved particle concentration measurement by
44   condensation particle counting methods (Jiang et al., 2011c; Kulmala et al., 2013). The time dependent
45   and size resolved particle concentrations are further used to infer the size resolved particle nucleation
46   and growth rates (Jiang et al., 2011c; Kuang et al., 2012; Kulmala et al., 2013; Lehtipalo et al., 2016;
47   Tröstl et al., 2016). Despite the recent advances, large uncertainties exist in the particle concentration
48   measurements in the sub-3 nm size range. The particle concentration measurement uncertainties

49 arise, for example, from low particle counting statistics (Jiang et al., 2011b), from chemical
50 composition dependent variation in the lowest threshold diameter of the particle counters (Jiang et
51 al., 2011b; Kangasluoma et al., 2014) or from unknown charging probabilities in the sub-3 nm size
52 range (Premnath et al., 2011). The uncertainties in the measured particle concentrations accumulate
53 into the derived parameters, such as the nucleation and growth rates.

54   Almost all of the recent experimental efforts to characterize sub-3 nm particle dynamics rely
55 on diethylene glycol (DEG) based condensation particle counters (CPCs) (Iida et al., 2009; Jiang et al.,
56 2011c; Kirkby et al., 2011; Kuang et al., 2012; Yu et al., 2012; Almeida et al., 2013; Kulmala et al., 2013;
57 Yu et al., 2014; Alanen et al., 2015; Kangasluoma et al., 2015; Bianchi et al., 2016; Kirkby et al., 2016;
58 Kontkanen et al., 2016; Nosko et al., 2016; Wang et al., 2016; Kontkanen et al., 2017; Wang et al.,
59 2017). However, a well-known challenge of a DEG based CPC is that the particle detection efficiency
60 at mobility diameters below 3 nm largely depends on the chemical composition of the particles.
61 Previously e.g. Jiang et al. (2011b), Kangasluoma et al. (2014) and Kangasluoma et al. (2016b) have
62 determined the detection efficiency of the DEG based CPCs in the laboratory for clusters of variable
63 chemical composition. The results show that the difference between the lowest and the highest d50
64 (diameter at which the detection efficiency is 50% of the plateau value) of the DEG based CPC can be
65 approximated to be at maximum 1 nm. This translates to an offset value of ± 0.5 nm in the d50 value,
66 if the particle chemical composition is completely unknown. However, this source of uncertainty can
67 be minimized almost to a negligible value, when the CPC is calibrated with the same type of particles
68 as sampled in the experiment (Kangasluoma et al., 2015). Unfortunately, this is currently not possible
69 for many applications, such as for atmospheric observations.

70   In addition to the uncertainties related to the particle composition dependent detection
71 probability, there are numerous other factors causing difficulties in the accurate measurement of the
72 sub-3 nm particle concentrations. The CPC calibrations rely on charged test particles as they can be
73 linked to the concentrations determined with electrometers, while there are no established
74 concentration reference instruments for electrically neutral sub-3 nm particles. Furthermore, there is
75 a lack of sources capable of producing electrically neutral and size selected particles with known
76 chemical composition. As heterogeneous nucleation of charged particles takes place at lower
77 supersaturation than that of neutral particles (Winkler et al., 2008; Kangasluoma et al., 2016b;
78 Kangasluoma et al., 2017), uncertainty in the d50 arises if charging state of the calibration aerosol is
79 not similar to the charging state of the measured aerosol. This source of uncertainty is most
80 pronounced when the measured aerosol is mostly electrically neutral and CPC calibration is conducted
81 with charged test particles. Also, if large but unknown fraction of the measured particles is charged,
82 the effect of charge on the d50 is difficult to take into account even with a proper calibration. Only
83 few sub-3 nm CPC calibrations with the size selected, electrically neutral particles have been
84 conducted so far (Kangasluoma et al., 2016b; Kangasluoma et al., 2017). They suggest an increase of
85 0.1 – 0.5 nm in the d50 for the neutral particles compared to the identical experiment with the charged
86 particles. Thus, if the effect of charge on the d50 is not known in a given experiment, one could assume
87 an increase of 0.3 nm to the d50, obtained from calibration with charged particles, which can be taken
88 into account in the data inversion. Thereby the d50 offset can be estimated as ± 0.2 nm, which covers
89 the range of d50 variation of current experimental data.

90   Brownian motion causes uncertainty in the sub-3 nm particle concentration measurements in
91 two ways. On one hand, the small particles are lost to sampling line walls very efficiently, which causes
92 uncertainty in the measured particle concentration. However, the size dependent losses can be
93 characterized experimentally and the effect can be corrected as long as there is at least some part of
94 the particles that penetrate through the sampling lines. The most straightforward way to overcome
95 this challenge is to use core sampling in the sampling line, which can increase the transmission of sub-
96 3 nm particles almost to unity (Kangasluoma et al., 2016a). On the other hand, the particle diffusion
97 hinders the particle size classification resolution (e.g. Stolzenburg and McMurry, 2008) of differential

98 mobility analyzers (DMAs). The challenges arise, when a DMA with a wide transfer function (Ω_{DMA})
99 relative to the sampled particle size distribution is used, as discussed later in this study.

100 Diffusion charging of aerosol particles larger than 10 nm in size is rather well understood (e.g.
101 Wiedensohler and Fissan, 1990), and similarly is chemical ionization via charge transfer at the
102 molecular scale (e.g. Eisele and Tanner, 1993; Lindinger et al., 1998). However, the transition from the
103 chemical charge transfer to the diffusion based charging taking place at the size scale of molecular
104 clusters is not well understood. Therefore, possibly a large source of uncertainty is related to the
105 charging efficiency of sub-3 nm particles and molecular clusters, which depend on the chemical
106 composition of the clusters themselves and the ions responsible for their charging. Overall, this
107 process is essential in the electrical mobility analysis based measurements. Few studies in the past
108 have probed the charging characteristics of the sub-3 nm particles. Alonso et al. (1997) presented
109 experimental data on bipolar charging probabilities of sub-3 nm particles, which underestimates the
110 charging probability by up to a factor of 2 from the Fuchs diffusion based charging theory. Premnath
111 et al. (2011) studied the charge transfer from the small clusters back to the vapor molecules, which is
112 not taken into account in the regularly used diffusion charging theories, and found out that the charge
113 transfer is dependent on both cluster size and chemistry. Due to a lack of experimental data the charge
114 transfer processes at cluster level are not well understood, and these effects are often not discussed
115 as a source of uncertainty in the sub-10 nm particle concentrations measurements. Alas, for the same
116 reason, our study does not discuss charging related uncertainties any further. This topic requires a
117 separate comprehensive analysis combining theoretical and experimental methods.

118 Lastly, uncertainties in the concentration obtained from CPC experiments can originate from
119 the number of counted particles. To probe this source of uncertainty, we assume that particle
120 sampling and counting is a Poisson process. A process needs to fulfil three requirements to be a
121 Poisson process (Bertsekas and Tsitsiklis, 2002):

122 1. Time homogeneity: at each time interval τ the probability to detect N counts needs to be
123 the same i.e. detection of a count is equally likely at all times.

124 2. The number of detected counts, N, during a time interval τ is independent of the history
125 of detected counts outside this interval τ, i.e. a detected count does not affect the
126 detection of another count.

127 3. During a short time interval: the probability to detect a count is roughly λτ (λ is the
128 counting rate), the probability to not detect any counts is roughly 1 − λτ, and when τ
129 becomes smaller, the probability to detect two or more counts becomes negligible.

130 In a Poisson process counting experiment, which is performed multiple times, the resulting number of
131 counts is a normal distribution around the mean value of count number. For a Poisson process the
132 distribution standard deviation, σ, equals to √N. The relative uncertainties ([%]) are obtained when σ
133 or √N are normalized with N. Generally, σ/N is defined as the statistical uncertainty, while √N/N is the
134 counting (Poisson) uncertainty. In Poisson process these are equal.

135 For CPC counting the conditions 1 and 2 are satisfied, if the particles in the sample air flow can
136 be considered to be distributed randomly (due to Brownian motion) and uniformly. The condition 3 is
137 satisfied, as there are no processes creating simultaneous counts i.e. each particle is sampled and
138 detected separately.

139 The purpose of this study is to numerically investigate the uncertainties related to the particle
140 counting with three different size distributions and four CPCs in five different case studies. The main
141 focus is placed upon the challenges arising from narrow input particle number size distributions, when
142 they are sampled with a theoretical CPC parametrized based on Kangasluoma et al. (2017) and
143 Vanhanen et al. (2011). The CPC counting statistics related uncertainty is first studied in a general CPC
144 counting experiment, and then examined based on a published state-of-the-art instrument utilizing
145 the DMA-CPC technique. The effect of non-ideality and offset in the d50 diameter on the detected
146 particle concentration are both studied in cases when a DMA is applied upstream of the CPC, and

147 without the DMA. Finally, the uncertainties in the particle sizing method utilizing supersaturation
148 scanning with a specific CPC are examined. The study presents the first comprehensive uncertainty
149 analysis on the sub-3 nm particle concentration measurements. Furthermore, suggestions are
150 provided for the future instrumental development to improve the accuracy of sub-3 nm particle
151 concentration measurements. It must be stressed that this study does not criticize any previous work,
152 nor claim anything on the reliability of any specific previous or forthcoming data. Rather, the previous
153 scientific works are appreciated as the inspiration for this analysis.

2 Methods

2.1 Instrumentation used in the numerical simulations

159   The online sub-3 nm particle sizing methods can be divided into two types of methods, named
160 here as a differential mobility analyzer – condensation particle counter (DMA-CPC) method and a
161 particle size magnifying (PSM) method. The DMA-CPC method functions as follows: the sampled
162 particles are first guided to an aerosol charger. The aerosol, which is assumed to be brought to charge
163 equilibrium in a charger (e.g. Wiedensohler and Fissan, 1990), is further guided to a DMA (Hewitt,
164 1957; Knutson and Whitby, 1975; Chen et al., 1998), leading to a charged and monodisperse particle
165 population downstream of the DMA. A CPC is used to count the number concentration of the particles.
166 This is a traditional differential mobility particle sizer (DMPS, e.g. Wiedensohler et al., 2012) method
167 used to monitor size resolved particle concentrations.

168   Sub-3 nm particle measurements can be performed using the DMA-CPC method with a TSI
169 nano DMA (Chen et al., 1998). We base our analysis on the system described in Jiang et al. (2011b), in
170 which the TSI nano DMA is operated at flow rates Q_a = 2 liters per minute (lpm) and Q_s = 20 lpm for
171 aerosol and sheath flows, respectively. The resolution (R) of the DMA (see Flagan, 1999) is defined as
172 the ratio between the selected mobility and the transfer function peak width (full width at half
173 maximum, FWHM) as follows: R = $Z/\Delta Z_{FWHM}$). In our case with the TSI nano DMA, the corresponding
174 resolution is 3 – 4 (Jiang et al., 2011a). The CPC used in Jiang et al. (2011b) was a modification from a
175 TSI ultrafine 3025A CPC (Stolzenburg and McMurry, 1991), in which the working fluid was changed
176 from butanol to DEG, and the original counting optics were removed and replaced by another follow-
177 up CPC (Jiang et al., 2011b; Kuang et al., 2012; Wimmer et al., 2013) as DEG is typically not able grow
178 the particles to large enough size to be detected with the optics. In the TSI ultrafine 3025A/3776 CPC
179 design the aerosol flow rate in the condenser is 0.3 lpm, out of which 0.03 lpm (in 3025A) or 0.05 lpm
180 (in 3776) contains the particles and is directed to the counting optics through a narrow capillary and
181 the rest is filtered and saturated sheath flow around the particle flow. This flow arrangement has two
182 implications on the analysis of this study: with the sheathed condenser design the d50 curve will be
183 steep as the particles are exposed to a rather constant supersaturation, while the dilution lowers the
184 counting statistics by a factor of 10 with the 3025A compared to TSI 3022, and by a factor of 33
185 compared to TSI 3772, where all of the sampled particles are directed to the optics with the flow rates
186 of 0.3 lpm and 1 lpm, respectively.

187   The PSM method refers to a mixing type CPC technology initiated by Okuyama et al. (1984),
188 and further developed by Seto et al. (1997) and Gamero-Castano and Fernández de la Mora (2000)
189 and their successors. In this method, the CPC is often named as a particle size magnifier as this
190 instrument was initially used to study the particle growth. The current commercial PSMs use DEG as a
191 working fluid which only initiates the particle growth (Vanhanen et al., 2011), thereby requiring
192 another CPC for the particle counting. The particle sizing in the PSM is based on the fact that
193 heterogeneous nucleation probability at a fixed supersaturation depends on the particle size (Fletcher,
194 1958). Thus, by scanning the supersaturation in the PSM, the particle size distributions can be inferred
195 from the total concentrations measured with the different d50 diameters (Lehtipalo et al., 2014). A

196 combination of Airmodus A10 PSM and A20 butanol CPC is commercially available as the A11 system
197 and the analysis of this study is performed for this setup.

198   A possible instrument in the future sub-3 nm particle studies is the recently published water
199 based CPC (Hering et al., 2016), which can achieve particle detection near 1 nm. Compared to a
200 conventional water CPC (Hering et al., 2005), the new versatile water CPC (vWCPC) has three
201 temperature stages instead of the previous two. With this kind of setup, it can reach supersaturations
202 high enough to detect particles as small as 1 nm. The vWCPC is a non-sheathed CPC, which
203 subsequently makes the d50 curve more flat relative to for example the original TSI 3025A design.

204   In this study we investigate the performance of three CPCs introduced above (TSI 3777,
205 Airmodus A11, and vWCPC), to detect particle concentration, and the DMA-CPC and the PSM method
206 to measure particle size distribution. In addition to the real CPCs, an ideal CPC with d50 at 1.5 nm is
207 included as a reference in the analysis to distinguish between the uncertainties related to the CPC d50
208 curve and other factors.

209   Figure 1 upper panel presents the d50 curves of the three CPCs, which are published in
210 Kangasluoma et al. (2017) for the vWCPC and 3777 and in Vanhanen et al. (2011) for the A11. The fits
211 to the curves are according to the following equation:

212

213 $\eta_{cpc}\left(d_p\right) = A * e^{\,(-e^{(-k*(dp-dp_0)})})}$ (1)

214

215 where A is the d50 curve plateau value height, d_{p0} is the diameter offset and k is a curvature
216 parameter.

217

218 **2.2 Test particle size distributions**

219

220 Three test particle size distributions (SDs) were selected for the study: one from ambient experiments
221 (SD1, Jiang et al., 2011c), one from a flow tube reactor experiment (SD2, Yu et al., 2012) and one from
222 an engine combustion exhaust emission study (SD3, Alanen et al., 2015) (Figure 1 lower panel). The
223 three SDs were chosen to represent the full variability in the number size distributions in the sub-3
224 nm size range to examine the effect of the sample SD on the uncertainty in the measured particle
225 concentrations. Therefore, these selected SDs contain only particles smaller than 10 nm, which is not
226 realistic e.g. for atmospheric conditions. However, larger Aitken or accumulation mode particles
227 would only increase the offset concentration detected by all the CPCs, which is not relevant for this
228 study as our focus is only on sub-3 nm sizes.

229   The following characteristics should be noted on the test size distributions: we have
230 normalized all the distributions to peak concentrations of unity for simplicity. Furthermore, in SD1 the
231 concentration decreases from the peak value of 1 at 1 nm to 0.01 at 2 nm, exhibiting a steep negative
232 concentration gradient as a function of particle size. Notably this gradient coincides with the size range
233 of the CPC d50 diameters. This kind of SD is typical for the systems where the clusters are constantly
234 formed from precursor vapors (Jiang et al., 2011c; Kulmala et al., 2013). Also, it should be noted that
235 in SD1 the concentration decreases towards zero below 1 nm, which is not realistic in ambient particle
236 SD. This does not, however, affect the results of the calculations as the CPCs of this study do not detect
237 any particles below 1 nm. In a similar manner, SD2 exhibits a steep concentration gradient, but in this
238 case the gradient is positive at the CPC d50 size range. The SDs similar to this can be observed in
239 particle reactors, where uniform and rapid particle formation and growth takes place, and the particles
240 have a uniform time to form and grow (Yu et al., 2012; Ezell et al., 2014). SD3 presents a much smaller
241 concentration gradient than the first two SDs with a peak concentration at 4 nm. These three size
242 distributions are used in three of the four case studies. In the second case study these SDs are not
243 used, but instead the SD required to achieve certain statistical uncertainty in the CPC counting is
244 calculated.

245

2.3 Data inversion

246

247

248 In the calculations presented in this study we focus on two parameters: the concentration detected
249 by the CPCs and the inverted concentration from the detected concentration, which gives the particle
250 SD when using the DMA-CPC or PSM method.

251

252 **CPC**
253 The concentration detected by the CPC (C_{tot}) directly monitoring a particular test SD was calculated
254 as:

255

$$C_{tot} = \int_0^\infty \frac{dC}{dd_x} * \eta_{CPC}(d_x) * dd_x \tag{2}$$

256

257 where dC/ddx ([arbitrary unit scaled to unity at peak concentration]) denotes the particle number size
258 distribution and η_{CPC}([%]) is the d50 curve for a given CPC shown in Figure 1. The uncertainties in C_{tot}
259 for different CPCs were investigated in case study 1 and 3 (see the next section).

260

261 **DMA-CPC**
262 In the DMA-CPC method the DMA transfer function was calculated according to Stolzenburg and
263 McMurry (2008). A concentration detected by the DMA-CPC system ($C_{det}(d_p)$, [arbitrary unit])
264 monitoring a test SD was calculated as:

265

$$C_{det}(d_p) = \int_0^\infty \frac{dC}{dd_x} * \eta_{CPC}(d_x) * \Omega_{DMA}(d_p, d_x) * dd_x \tag{3}$$

266

267 where Ω_{DMA} ([%]) is the DMA transfer function. From the $C_{det}(d_p)$ the inverted SD, $C_{inv}(d_p)$ ([arbitrary
268 unit, same scale as of C])*, is calculated as:

269

$$C_{inv}(d_p) = \frac{C_{det}(d_p)}{\eta_{CPC}(d_p) * A * \int_0^\infty \Omega_{DMA}(d_p, d_x)dd_x} \tag{4}$$

270

271 where η_{CPC} is the detection efficiency of the CPC at a given diameter, $\int_0^\infty \Omega_{DMA}$ is the integral over the
272 DMA transfer function and A is the d50 curve plateau value. We assume all particles to be singly
273 charged, as in the sub-3 nm size range the probability of double or more charging is close to zero
274 (Wiedensohler and Fissan, 1990). Note that in the inversion, the use of η_{CPC} and Ω_{DMA} as single values
275 contain the assumption that the SD does not significantly change over the size range where the d50
276 curve increases from 0 to A, or in the size range of the Ω_{DMA}. On the contrary, the $C_{det}(d_p)$ takes into
277 account the shape of the SD, d50 and Ω_{DMA}. This is the case in all real DMPS experiments too. In cases
278 studies 3 and 4 we examine the validity of this assumption by sampling the strongly varying SDs as a
279 function of the particle size.
280 When a CPC of a DMPS system records particle counts, the following parameters need to be
281 taken into account in the inversion: particle sampling losses, charging probability, DMA penetration
282 and CPC detection efficiency, the product of which is the particle size dependent total penetration
283 ($P_{tot}(d_p)$) of the system. In this study, we follow the DMPS system presented in Jiang et al. (2011b). The
284 total penetration of this system is depicted in Figure 2. As shown in the introduction part, the counting

285 statistics can be assumed to follow Poisson statistics, i.e. the number of counts in a given time interval
286 is known on average, but the time interval between two counts is random. Thus, during a fixed time
287 period the obtained number of counts can deviate from the average. When many identical counting
288 experiments are conducted, the obtained counts follow a normal distribution. The standard deviation
289 of this distribution describes the statistical uncertainty of the counting experiment. It can be shown
290 that the counting uncertainty, which follows Poisson statistics is $\sqrt{N}/N$ where N is the number of
291 counts (see Figure 3). For example, 10 and 100 counts counted by the CPC yields ±31% and ±10%
292 counting uncertainty, respectively. The individual counts from particles detected by the CPC of a DMPS
293 system can be calculated from

$$N = C_{SD}(d_p) * P_{tot}(d_p) * t * Q_o \tag{5}$$

297 where $C_{SD}(d_p)$ is the sampled concentration of particles, $P_{tot}(d_p)$ is the total penetration of the DMPS
298 system, t is the counting time i.e. the time the DMA spends at one voltage, and Q_o is the flow rate
299 through the optical detector of the CPC. This system is examined in the case study 2.

PSM

302 The inversion for the PSM method follows the methodology presented in Lehtipalo et al. (2014).
303 However, the difference in our inversion is that we use experimentally defined Ω_{PSM}s as compared to
304 the selected Ω_{PSM} shapes of Lehtipalo et al. (2014). Figure 4 (left hand side panel) shows the PSM
305 calibration, which is obtained by feeding size selected tungsten oxide particles to the PSM, and
306 scanning the supersaturation by scanning the saturator flow rate (Q_{sat}). The calibration curves are
307 normalized to unity at Q_{sat} = 1 lpm. From the normalized curves the Ω_{PSM}s are obtained by subtracting
308 the calibration curves from each other so that the obtained size bins are 1.1–1.2 nm, 1.2–1.3 nm and
309 so on. To these Ω_{PSM}s, Gaussian curves are fitted (Figure 4 right hand side panel). Q_{sat} is converted to
310 diameter (x-axis in Figure 4 right hand side panel) by finding out Q_{sat} for which the detection efficiency
311 is 50% of the maximum value for each diameter. The diameter for each size bin was selected as the
312 diameter corresponding the maximum value of each Ω_{PSM}. These Ω_{PSM}s can be readily used in the
313 calculations similarly as the DMA Ωs. The concentration detected by the PSM method is given by

$$C_{det}(d_p) = \int_0^\infty \frac{dC}{dd_x} * \Omega_{PSM}(d_p, d_x) * dd_x \tag{6}$$

316 From $C_{det}(d_p)$, the inverted concentration is calculated as

$$C_{inv}(d_p) = \frac{C_{det}(d_p)}{\int_0^\infty \Omega_{PSM}(d_p, d_x)dd_x} \tag{7}$$

319 In case study 5 we examine the PSM inversion, and the effect of diameter offset in Ω_{PSM} to the inverted
320 SDs.

2.4 Case studies

324 Five case studies were performed to address various aspects affecting the uncertainties in measured
325 sub-3 nm particle concentrations. In cases 1 and 2 we examine statistical uncertainties of CPC and
326 DMPS counting, and briefly discuss the statistical uncertainties related to cases 3-5. In cases 3-5 the
327 uncertainty in the measured particle concentrations was studied 1) by assuming well-known d50
328 curves or 2) by inserting ± 0.5 nm offset to the d50 curve. In the calculations in which no d50 offset

329 was assumed, the d50s are the ones presented in Figure 1. In the calculations in which the offset is
330 inserted to the d50 curve, it is conducted so that the initial d50 curve is shifted by + 0.5 nm, which is
331 taken as the reference d50 curve, and then ± 0.5 nm offset is inserted to this reference curve. The
332 reasoning for this is that the d50s presented here (and in the manufacturer brochures) are the best
333 case curves i.e. the lowest d50 values obtained using particles that are easily detected with the
334 instrument. The offset value of ± 0.5 nm is taken from our previous studies (Kangasluoma et al., 2014;
335 Kangasluoma et al., 2016b) to reflect the case where composition of the sampled particles is unknown.
336 In real experiments the d50 offset can be larger, for example ±0.75 nm, if the effect of charge and
337 relative humidity are not considered, but also smaller (even negligible) if the particle composition and
338 charging state are known and taken into account in the instrument calibration. For this study, the
339 absolute value of the d50 offset is important in the sense that if it was larger, the resulting
340 uncertainties in the detected particle concentrations would be larger, and vice versa. It must be
341 highlighted that the uncertainty can be narrowed down by a proper instrument calibration as shown
342 for example in Kangasluoma et al. (2015), and data presented here do not represent any specific
343 experiment.

344

345 **Case 1: Statistical uncertainty in CPC sampling**
346 We performed Monte Carlo simulations to test the validity of our subsequent non-statistical analysis.
347 In the simplest case, the real CPCs sample a particle distribution representing the SD1. The number of
348 sampled particles from the SD, N, was set to 10, 100, 1000, 10000 and 100000 on average. As sampling
349 of particles in our study is assumed to be a Poisson process, in each simulation N is a random number
350 from normal distribution around N with $\sigma = \sqrt{N}$. The probability of detection for each sampled particle
351 was according to the CPC d50 curve, with uniform detection probability. This simulation was
352 conducted 10000 times for each N, and the number of counted particles was analysed. From the
353 distribution of counted particles the uncertainty can be calculated in two ways: statistical uncertainty
354 as σ/N, or Poisson counting uncertainty as $\sqrt{N}/N$.

355

356 **Case 2: DMA-CPC statistical uncertainty**
357 In this case study the performance of the complete DMPS system, described in Section 2.1, with
358 respect to counting of sub-3 nm particles and counting statistics is examined. The only studied
359 uncertainty is the counting uncertainty, and other variables are assumed to be well-known. In this
360 case study, we determine which sampled size distribution yields counting uncertainty smaller than
361 5%, 15% and 50%, which correspond to 400, 44 and 4 counts, respectively (Figure 3). The SD is directly
362 obtained from Eq. 5 by solving it for $C_{SD}(d_p)$. In the calculations t is set to 15 s and Q_o to 0.03 lpm. The
363 value of t is calculated from Jiang et al. (2011b) assuming constant t at each DMA voltage. In many
364 DMPS systems t might not be constant as a function of size but the counting time is increased for the
365 smallest particles. However, the results from this study scale linearly with t, i.e. doubling t reduces the
366 required concentration to half.

367

368 **Case 3: CPC sampling**
369 In the third case study the four CPCs (3777, A11, vWCPC, and ideal CPC) directly sample the three SDs
370 (Eq. 2), first assuming no error in the d50 curve, and then including a ±0.5 nm offset to the d50 curve
371 as explained in Section 2.4. When no offset is assumed, the parameters of interest are the ratio
372 between the detected concentration and the real concentration above the nominal d50, and the
373 fraction of the detected particles that are smaller than the nominal d50 of a CPC. When the ±0.5 nm
374 offset is inserted to the d50, the detected concentration is compared to a number which the CPC
375 should detect in an ideal case, that is, the concentration above the nominal d50 in the SD.

376

377 **Case 4: DMA-CPC sampling**

378 In the fourth case study a DMA is placed upstream of the CPC and the DMA-CPC system samples the
379 test SDs with the four different CPCs (Eqs. 3 and 4). We do not consider any uncertainties related to
380 particle sampling or charging. Similar analysis is performed as in the second case study: firstly the
381 inverted concentrations are analyzed with respect to the initial SD assuming no error in the d50, and
382 secondly ±0.5 nm offset is added to the d50. The inverted concentrations are compared to the initial
383 SDs, the parameter of interest being the ratio of these two.
384
385 **Case 5: PSM sampling**
386 In the last case study, the uncertainties related to the PSM method are examined similarly as in the
387 cases 3 and 4 by using Eqs. (6) and (7). Firstly the deviations in the inverted concentrations from the
388 initial SDs are studied, when no error in the d50 is assumed, and secondly the Ω_{PSM}s of the A11 are
389 exposed to an offset of ±0.5 nm. It is assumed that all the Ω_{PSM}s shift with a constant value of ±0.5 nm,
390 which, however, might not be a completely accurate assumption.
391
392 **3 Results and discussion**
393
394 **3.1 Case 1: Statistical uncertainty in CPC sampling**
395
396 An example figure of the first simulation is shown in Figure 5, the top panel showing one size
397 distribution with N = 1000 (on average) where on top the SD1 and CPC d50 curves are plotted. The
398 second panel presents the counted particle frequency for the 10000 simulations for the vWCPC with
399 N = 1000. By calculating the two uncertainties, statistical and counting, from the distributions such as
400 the one shown in the second panel, we obtain numbers in the Table 1. The uncertainty of the counted
401 particles follows Poisson counting uncertainty as shown in the Table 1 (similar values for σ/N and
402 √N/N), so, the uncertainty is only dependent on the number of counted particles. This is expected
403 from the properties of the Poisson process: if we consider only particle of one size, its detection can
404 be assumed to follow Poisson statistics. If we consider particles of two different sizes with unequal
405 detection rates which are independent of each other, their sum still follows Poisson statistics. This can
406 be generalized to *n* different independent sizes of particles with unequal detection rates, the sum of
407 which follows Poisson statistics. Based on this, we can make a simple calculation for a usual CPC
408 counting experiment: let us assume CPC optics flow rate of 1 lpm, counting time of 1 s and sampled
409 concentration of 100 particles cm^{-3}. This gives us counted particles of N = 1660 (on average) and
410 counting uncertainty of ±2.5%. Based on the relatively good counting statistics in a normal CPC
411 counting experiments, we can conclude that the counting, and thus, statistical uncertainties are quite
412 low in most CPC counting experiments. Possibly excluded situations are CPCs with very low optics flow
413 rates or/and environments with very low particle concentrations, such as artic areas or clean room
414 facilities. In these cases the counting statistics are easily improved by longer counting time.
415 Importantly, the previous still holds when the particles are sampled with a DMPS system: the
416 sum of particles with different detection rates (inside the width of a DMA transfer function originating
417 from different charging and DMA transmission probabilities, and changing size distribution) obey the
418 Poisson process and statistics. The fact that particle counting with both a CPC and a DMPS follow
419 Poisson statistics generalizes the statistical uncertainties of concentration measurements to Poisson
420 uncertainty. In general, this is useful observation, since very seldom the measured processes are slow
421 enough to obtain sufficient amount of scans with a DMPS system to calculate the σ/N, and the number
422 of counted particles in the DMPS system is not often high enough to neglect the counting uncertainties
423 for a single measurement.
424 Tables 2 and 3 list the statistical uncertainties obtained for the parameters listed in Tables 4
425 and 5 for SD1 at various N values. Table 4 lists the ratio of detected concentration and true
426 concentration above the CPC d50, while Table 5 lists the ratio of detected concentration and detected
427 concentration below the CPC d50. We selected these two parameters to describe the CPC

428 performance in measuring particle concentrations at sizes close to the CPC d50. Statistical
429 uncertainties of these parameters do not follow Poisson uncertainty, as they are calculated from two
430 variables that are dependent on each other. Based on the current study we cannot generalize these
431 uncertainties quantitatively, but only qualitatively as follows: the uncertainties are lower when the
432 number of counted particles is higher. On the other hand, the uncertainties are lower when the CPC
433 d50 is the steeper or the particle SD is flatter. The former is trivial and observed in Tables 2 and 3. The
434 latter can be reasoned as follows: a counting experiment with an ideal CPC does not suffer from the
435 non-idealities of the parameters of Tables 4 and 5, and the steeper the d50 curve, the smaller the
436 possibility of counting particles below the nominal d50. Similarly, the steeper the SD, the more
437 important parameter the CPC d50 is in determining the particle concentration accurately, as is obvious
438 from later parts of this study.
439   We do not study the magnitudes or uncertainties of these uncertainties that do not follow
440 Poisson uncertainties more deeply because they are very case dependent and depend strongly on the
441 SD shape, d50 shape, counted particle number and factors causing d50 offset. Due to the previous,
442 more general approach nor more deep analysis has not been done also for the numbers obtained in
443 Figures 8 and 10, and in Tables 6a and 6b. However, we can conclude that, at least for such parameters
444 listed in Tables 4 and 5, if number of detected particles is 1e4 or more, the statistical uncertainties of
445 the parameters are less than 5%. This is most probably a good estimate for the data of Figures 8 and
446 10, and Tables 6a and 6b, since those parameters are calculated from two similar (but not
447 independent) variables as in Tables 2 and 3.
448   All in all, in most normal CPC and DMPS experiments, and our cases 3 and 5, the statistical
449 uncertainties can be assumed to be equal to Poisson uncertainty, and all derivative parameters of this
450 study to have statistical uncertainties smaller than 5% if number of counted particles is more than
451 1e4.
452
453 **3.2 Case 2: DMA-CPC counting uncertainty**
454
455 In the third case study, we assume that all the instrumental parameters are well-known, and we only
456 examine the uncertainty related to counting statistics in the DMA-CPC system. The DMPS system
457 follows the performance of the only published DMPS system measuring particles down to 1 nm by
458 Jiang et al. (2011b) (Figure 2). Figure 6 shows the particle SDs with the concentrations required to
459 achieve 4, 44 and 400 counts to the CPC of the examined system. These counts represent the number
460 of counts in any counting experiment which yield counting uncertainties smaller than 50%, 15% and
461 5%. It can be seen from the figure that the studied DMPS system requires the sampled particle
462 concentration of approximately 1e7 cm^{-3} at 1 nm to achieve the counting uncertainty smaller than 5%.
463 At 3 nm, the respective concentration is approximately 1e5 cm^{-3}. To achieve the counting uncertainties
464 of smaller than 15% and 50%, the respective concentrations are approximately one and two orders of
465 magnitudes lower than the ones for 5%. This result clearly implies that to obtain statistically reliable
466 data (or any data at all), one needs very high particle concentrations at the DMPS system inlet. There
467 exist at least two methods to rather easily increase the counting statistics of the studied DMPS system:
468 using a detector with a higher optics flow rate and optimizing sampling line penetration. For example,
469 the TSI 3777 (Kangasluoma et al., 2017) offers the detected flow rate of 0.15 lpm and the A11 system
470 the flow rate of 1 lpm, which enable better counting statistics by a factor of 5 and 33, respectively,
471 compared to the TSI 3025A. The sampling system presented in Kangasluoma et al. (2016a) practically
472 removes inlet line losses, producing almost a tenfold increase to the signal at 1 nm. By implementing
473 the improved counting statistics by a factor of 33 by replacing the 3025A with an A11 and improved
474 sampling line, the required concentrations presented in Figure 6 would be approximately two orders
475 of magnitude smaller. Further improvements would be obtained by improving the transmission of the
476 DMA, or by improving the charging efficiency, which at the current stage will require more
477 fundamental research.

478

3.3 Case 3: CPC sampling

480

For the three studied SDs, the ratios of the detected concentration to the real concentration above the d50 of each CPCs are listed in Table 4. The errors in the detected concentrations, indicated as the ratio between the CPC response to the ideal performance (ratio's deviation from unity), result from the changing size distribution at the size range where the d50 increases from 0 to A. Therefore, the errors are the largest (-12% to 272%) for the vWCPC as its d50 curve increases from 0 to A in the largest diameter range (see Fig. 1). The d50 curves of the 3777 and A11 are similarly steep but placed at different concentration gradient of the SDs. Because the concentration gradient is larger at the d50 of the 3777 compared to the A11, the errors are also larger for the 3777 (-4% – 32%) than for the A11 (-1% or less).

The fractions of the detected particles that are smaller than the nominal d50 of CPC, are given in Table 5 for different SDs. As expected, the ideal CPC does not detect anything below its d50 but the real CPCs detect particles that are smaller than the nominal d50 of a CPC due to the non-ideal d50 curves. The smallest fractions (less than 2%) are observed for the SD3 in which the concentration gradient is positive and relatively small at the size of the CPC d50s, and most of the particles in the SD are larger than the d50 values. For the SD2 with a larger but positive concentration gradient at the d50 sizes, the fractions are also relatively low, less than 10%. However, when the gradient is large and negative, as is the case for SD1, a significant fraction of the detected particles is below the nominal d50 values. For vWCPC the fraction of the particles detected below the d50 value is the highest (67%) as the d50 curve reaches to much smaller diameters as its nominal d50 value. The d50 curves of 3777 and A11 exhibit similar steepness, but as the d50 of the 3777 is at the region of higher concentration gradient for the SD1, the fraction of the particles detected below d50 is larger (37%) than the value of A11 (12%) (Table 5). These results imply that non-idealities of the d50 curve can cause significant measurement error, particularly in the cases when the SD is narrow. In the worst case it can cause either an overestimation up to some hundred percent (SD1) or an underestimation of some ten percent (SD2) (Tables 4 and 5).

Next, ±0.5 nm error was applied to the d50 curve, and the detected concentrations are compared to the real concentration above the nominal, correct d50 values. Tables 6a and 6b present the concentration ratios for the d50 offsets of +0.5 nm and -0.5 nm, respectively. Errors in the detected concentrations are again the smallest for the SD3, approximately ±15%, due to the smallest concentration gradient and the fact that most particles in the SD are larger than the d50s. For SD2, in which the peak concentration is close to the d50 values, the ± 0.5 nm error in d50 curve causes errors of approximately -70% to +130% to the detected concentrations. The errors in the detected concentration are the largest for the SD1, ranging from -98% to > 1000%. This is because in SD1 there is a strong negative concentration gradient in the size range of the d50s of all the CPCs. The observed errors in the detected concentrations imply strongly that the knowledge on the d50 is crucial when determining the particle concentrations in systems where particle formation takes place, producing steep particle size distributions. The magnitude of the error is determined by the combination of how CPC d50 is located relative to the SD and the shape of the d50 curve. The stronger the concentration gradient is, more uncertainty in the detected concentration is induced, if d50 is not exactly known. Most importantly, universal uncertainty in the detected concentration cannot be given even if the uncertainty in the d50 can be known, as the concentration uncertainty always depends on the sampled particle SD.

523

3.4 Case 4: DMA-CPC sampling

525

526 In case study 4 a Ω_{DMA} is included in between the particle SD and CPC, and inverted concentrations are
527 studied. The inverted concentrations are limited to values where the detection efficiency of the CPC
528 is larger than 5% and where the size distribution is more than 0.1% from the peak value. This is to
529 avoid the most extreme and uncertain values, which probably would not be used in a real experiment
530 either. Figures 7a-c present the inverted SDs and the ratios of inverted SDs to the initial SD for different
531 SDs with all CPCs. In these plots the d50 is assumed to be known, and all errors in the inverted
532 concentrations arise from the fact that the particle concentration changes in the size range of the Ω_{DMA}
533 and d50 curve.

534 From Figure 7 it can be observed that the ideal CPC underestimates the concentration close
535 to the d50 value for all the SDs. This is because the DMA transmits also particles smaller than the d50,
536 which are not detected by the CPC. At the sizes where all the particles are larger than the ideal CPC
537 d50, the ideal CPC, like all other CPCs, overestimates the detected concentration by approximately 0
538 – 15%. This results from the fact that the particle concentration in the SD decreases exponentially as
539 a function of size, and therefore the concentration at the Ω_{DMA} maximum value does not represent
540 the average concentration over the whole Ω_{DMA} width. For the real CPCs, two processes are competing
541 below the CPC d50 value: the concentration is underestimated because particles smaller than the d50
542 are transmitted through the DMA, since the concentration gradient is strongly negative in the SD at
543 the d50 size. Simultaneously the concentration is overestimated because the particles larger than the
544 d50 size are also transmitted, and they are detected at a higher probability than the value of $\eta_{CPC,dp}$
545 (CPC detection efficiency at a given diameter) used in the inversion. Correction to the detected particle
546 concentration due to $\eta_{CPC,dp}$ increases with the decreasing particle size, and the net effect leads to the
547 overestimated particle concentration. This overestimation is most pronounced for the SDs 2 and 3 in
548 which the concentration gradient at the sizes of d50 is positive, and therefore relatively more particles
549 larger than the d50 are transmitted through the DMA.

550 Thus, in the case of the DMA-CPC system the instrumental non-idealities alone can cause
551 significant error in the detected concentration. In our calculations, these errors range from -60% up
552 to 560% depending on the diameter, the initial SD and the characteristics of the CPC. The largest
553 overestimations are associated to diameters where the CPC detection efficiency is lower than 0.5*A
554 (half of the d50 curve plateau value). The overestimation is smaller for the vWCPC than for the 3777
555 and A11 because its d50 is the least steep. As mentioned above, for these calculations we used only
556 diameters at which the CPC detection efficiency was larger than 5%. However, to avoid the observed
557 underestimation and overestimation problems in data inversion, using diameters at which the CPC
558 detection efficiency is larger than 0.9*A is suggested. At diameters where $\eta_{CPC} > 0.9*A$, the error was
559 smaller than 15% for SD1 and smaller than 2% for SD2 and SD3. The high uncertainties arise again
560 from the steep SDs as a function of particle size. The magnitude of the errors cannot be estimated, if
561 the size distribution is not known before the inversion routine, which is always the case in real
562 experiments.

563 Next, ±0.5 nm error is introduced to the d50 values of the CPCs. The ratios of inverted
564 concentration to the initial size distribution in this case are shown in Figures 8a-c. The observed
565 deviations in the inverted concentration from the real concentration follow rather similar patterns for
566 all the CPCs and SDs. The uncertainties range from -100% to > 1000% and they are again most
567 pronounced for the SD1 due to the strong negative concentration gradient at the d50 sizes. These
568 results further show that if the d50 of a CPC is not exactly known for the studied system, the safest
569 way is to use a DMA-CPC system that starts from a diameter where the CPC detection efficiency is
570 above 90% of the plateau value for the worst case d50. With the DEG based CPCs this limit lies
571 somewhere around 2 – 3 nm (Kangasluoma et al., 2014).

572

573

574 **3.5 Case 5: PSM sampling**

575

576   In the last case study, we investigate the performance of the A11 method in retrieving the SDs by
577   means of scanning the supersaturation. Following the similar analysis as in the case studies 3 and 24
578   we first analyze the inversion without uncertainties in the Ω_{PSM}s, and subsequently add a ±0.5 nm error
579   to the Ω_{PSM}s presented in Figure 4. The analysis is again limited to the SD diameters, where the
580   concentration is larger than 0.1% of the peak concentration. As in the case of the DMA-CPC inversion,
581   the PSM inversion includes uncertainties resulting from the fact that the particle concentration
582   changes significantly within the width of a Ω_{PSM}. As seen from Figure 9, SD1 is overestimated at 2 nm
583   while SD2 is underestimated at this size. This is due to Ω_{PSM}s which are skewed toward larger sizes. On
584   the other hand, the inversion of the rather flat SD3 includes relatively small errors. The errors in the
585   inverted concentrations ranged from -15% to +70%.

586   The error of ± 0.5 nm in the Ω_{PSM}s causes error in the measured concentrations at all sizes in
587   the inverted concentrations for the PSM method, while for the DMA-CPC the errors are only at the
588   size range close to the CPC d50 (see Section 3.2). Thus, in the case of the PSM method, the initial SD
589   mostly defines the magnitude of uncertainty in the inverted concentration (Figures 9 a-c). The largest
590   errors in the inverted concentrations are observed for the SD1, ranging from -100% up to 5000%. The
591   concentration can also be under- and overestimated for a single SD as shown for SD2 when there is
592   +0.5 nm offset in the Ω_{PSM}s. These, rather large, uncertainties are obtained because the inverted
593   concentration with shifted Ω_{PSM} is directly compared to the initial size distribution. It corresponds to
594   the case in which the instrument user needs a size classified concentration at a given (mobility)
595   diameter. Estimating the associated uncertainties for a given experiment is challenging because the
596   uncertainty depends on the initial SD. In this case study, all the uncertainties are assumed to be in the
597   particle concentration, which leads to very high uncertainties. Therefore, a more convenient approach
598   in the PSM method would be to include only counting and other experimental uncertainties in the
599   concentration uncertainty, and include the Ω_{PSM} related (particle composition, charge and sample flow
600   relative humidity) uncertainty in the size bin uncertainty. In the following nucleation and growth rate
601   calculations the size bin uncertainty would be directly the corresponding size uncertainty of the size
602   at which the nucleation or growth rate was calculated. In our case study, this would mean that instead
603   of having uncertainty from -100% to 5000% in the concentration with exact diameter, the
604   concentration uncertainty would be from -15% to 70% and the diameter uncertainty ±0.5 nm. In this
605   case the SDs inverted from PSM method would be supersaturation equivalent diameters, which would
606   make data intercomparison more straightforward. On the other hand, this could complicate further
607   analysis, such as interpreting particle formation and growth rates calculated from the concentrations
608   or the comparison between the concentrations measured with the PSM and other instruments.

609

610   **4 Conclusions**

611

612   In this study, the uncertainties in the sub-3 nm particle concentration measurement were examined.
613   Several parameters that affect the accuracy of the measurement were identified, including the initial
614   size distribution (SD), the steepness of the detection efficiency (d50) curve of the detector, the d50
615   accuracy with respect to the particle composition and charge (how well the CPC calibration test
616   aerosol represents the measured aerosol), and detector counting statistics. Based on the analysis, the
617   following conclusions can be drawn:

618   1) In all CPC and DMPS experiments the Poisson statistics uncertainty ($\sqrt{N}/N$) describes the
619   statistical uncertainty of the counted particles.
620   2) Achieving the counting uncertainty smaller than 5% with the studied DMPS system requires
621   high particle concentrations (> 1e5 cm^{-3}), which are not present in many systems.

3) CPCs can sample particles smaller than their nominal d50 diameter due to non-ideal d50 curve, which, depending on the sample SD can lead to overestimation or underestimation of the particle concentration. In our cases concentration error was in the range of -12% to 272%.

4) In the data inversion, using a single value for the DMA and PSM transfer functions (Ω_{DMA} and Ω_{PSM}) and CPC detection efficiency (η) is inevitable but it causes errors in the inverted concentrations. This results from the fact that the particle concentration can change significantly within the width of a Ω_{DMA} and Ω_{PSM}.

5) The steeper function of particle size the initial SD is, the larger the uncertainties in the concentration measurement are.

6) The largest uncertainties in the inverted concentrations with the DMA-CPC can be avoided by limiting the size range of the instrument only to diameters where the CPC detection efficiency is more than 90% of the plateau value. By using smaller CPC detection efficiency values than 90% the concentration error can be up to 500% due to instrumental non-idealities.

7) If the properties of the sampled particles are unknown, the largest uncertainties in the measured concentrations are associated in the PSM sizing method (in our cases from -100% to 5000% in the whole sizing range with ±0.5 nm d50 uncertainty), since the transfer functions, Ω_{PSM}s, are directly exposed to the uncertainty in the η. With the DMA-CPC method unknown particle properties cause uncertainty to the measured concentration only in the size range close to the d50 (in our cases from -100% to 1000% with ±0.5 nm d50 uncertainty).

8) Uncertainties are always case dependent

Future research to reduce the simulated uncertainties presented above, should focus on:

1) Designing CPCs with steeper d50 curves.

2) Finding nontoxic CPC working fluid capable of sub-3 nm particle detection and with a minimal composition and charge dependency, and homogeneous droplet production.

3) Building DMAs with a higher sizing resolution (R > 5) with reasonable transmission which are applicable to field experiments.

4) Improving DMPS counting statistics by
   a. Using CPCs with larger optics flow rates.
   b. Minimizing the sampling losses.

5) Studying sub-3 nm charging efficiency

Further, the implications of the particle concentration measurement uncertainties on the derivative parameters, such as the particle nucleation and growth rate (Kulmala et al., 2012), should be studied.
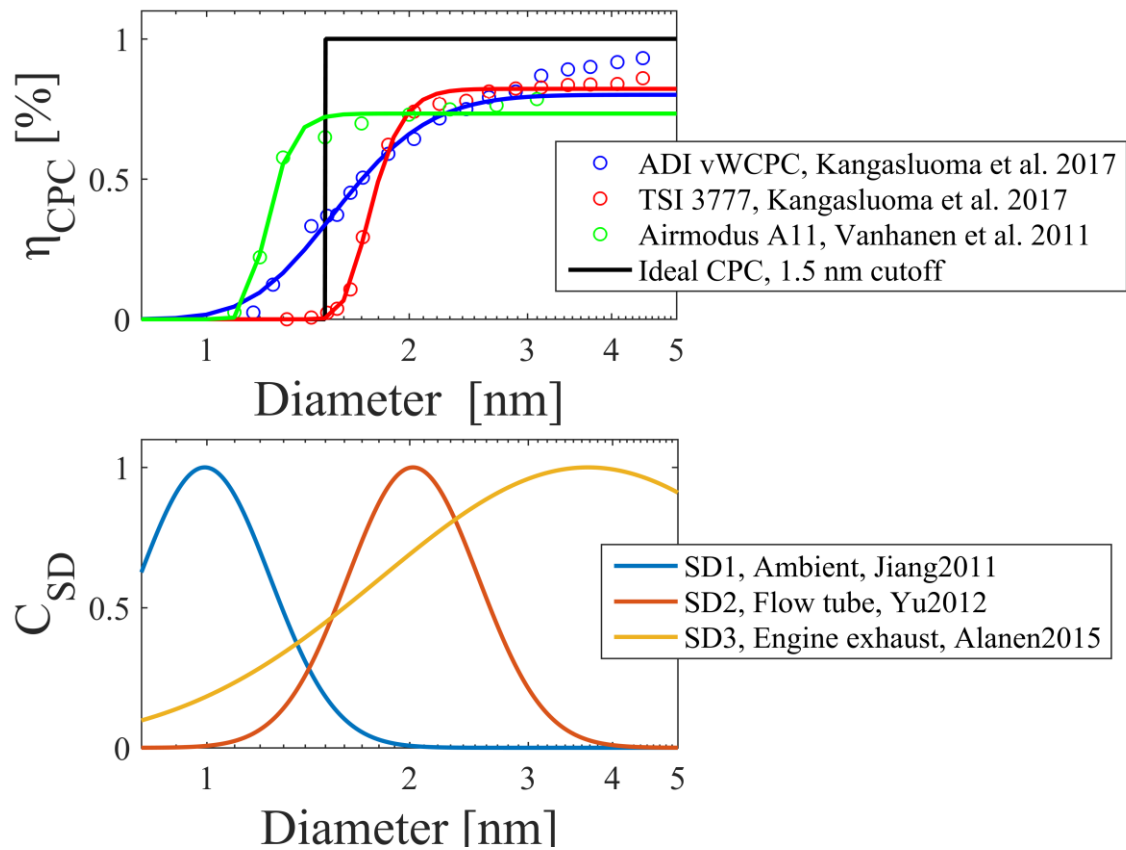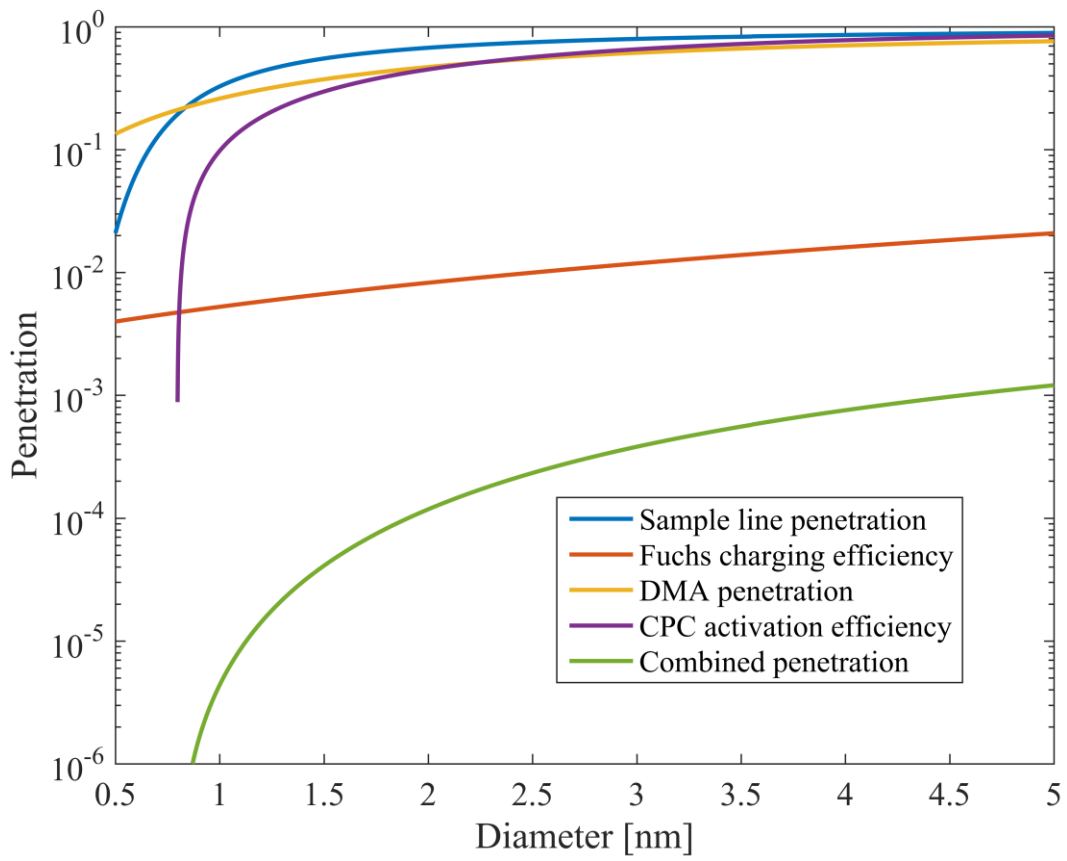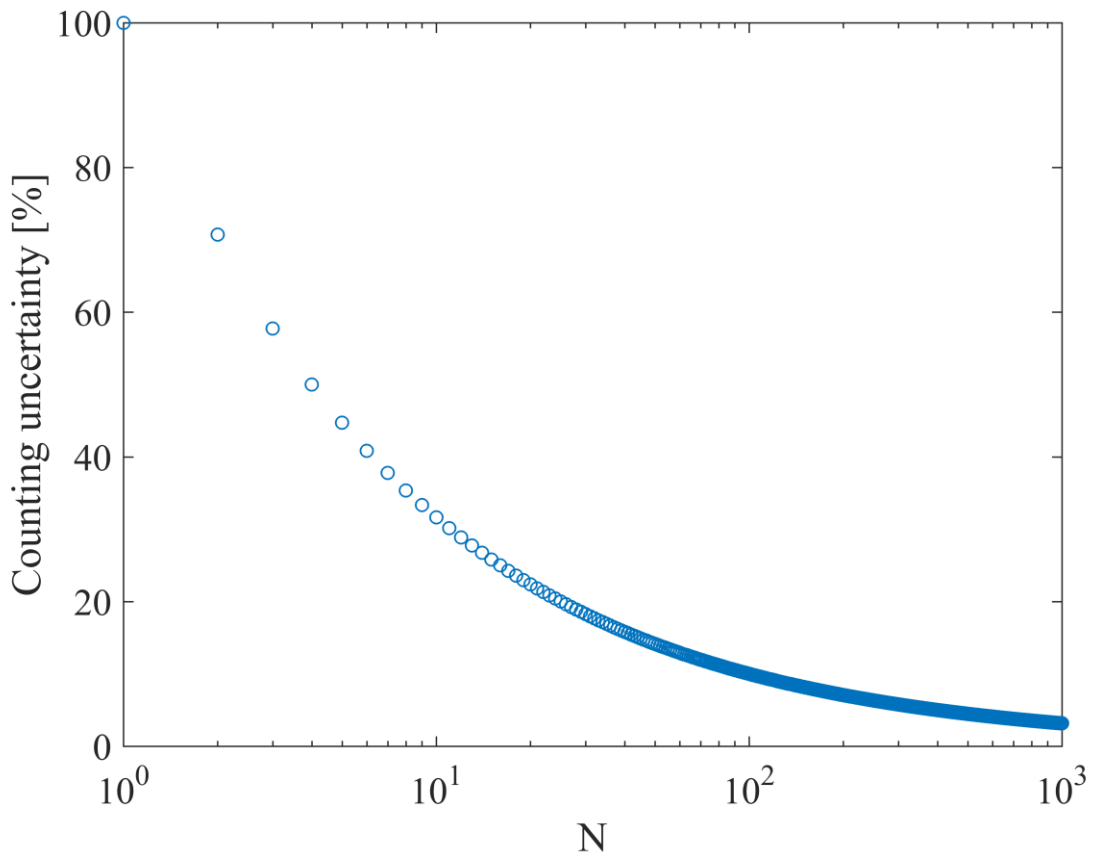
Acknowledgements

663
664 Figure 1. The CPC d50 curves and test particle size distributions. Concentration unit for the size
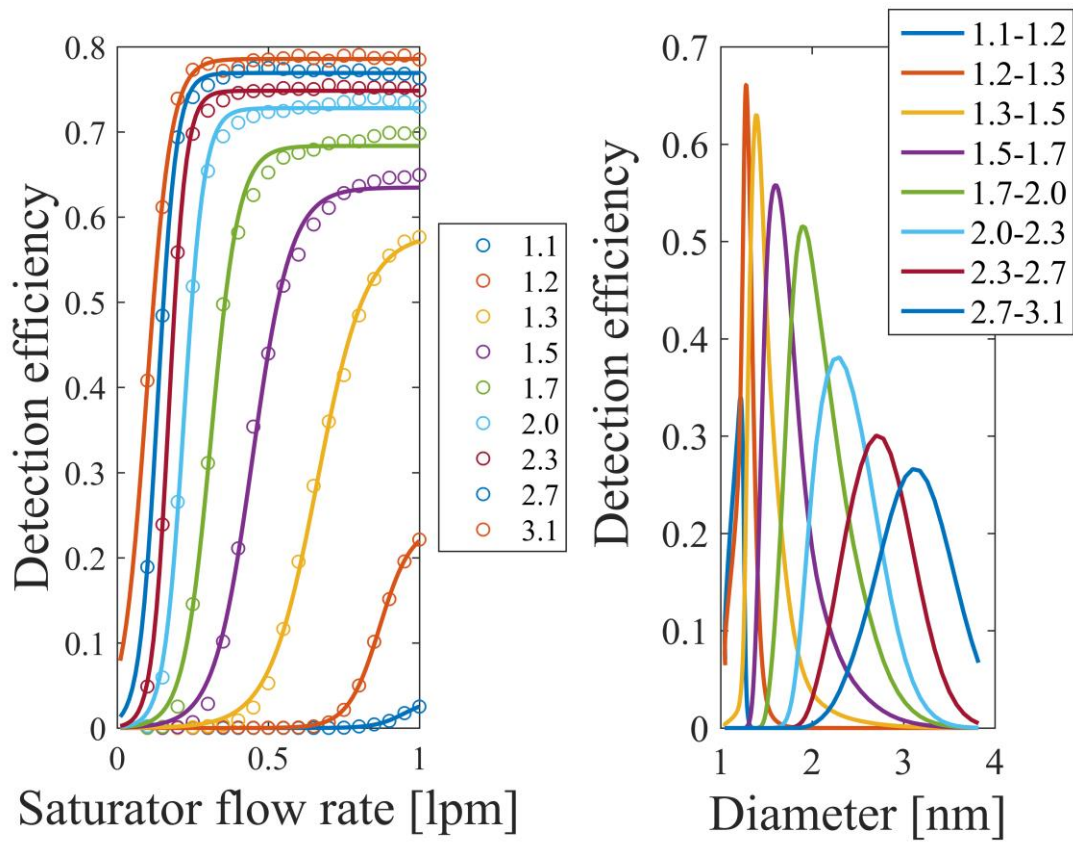665 distributions is arbitrary.

666

667   Figure 2. Penetrations of the DMPS system in case study 3.
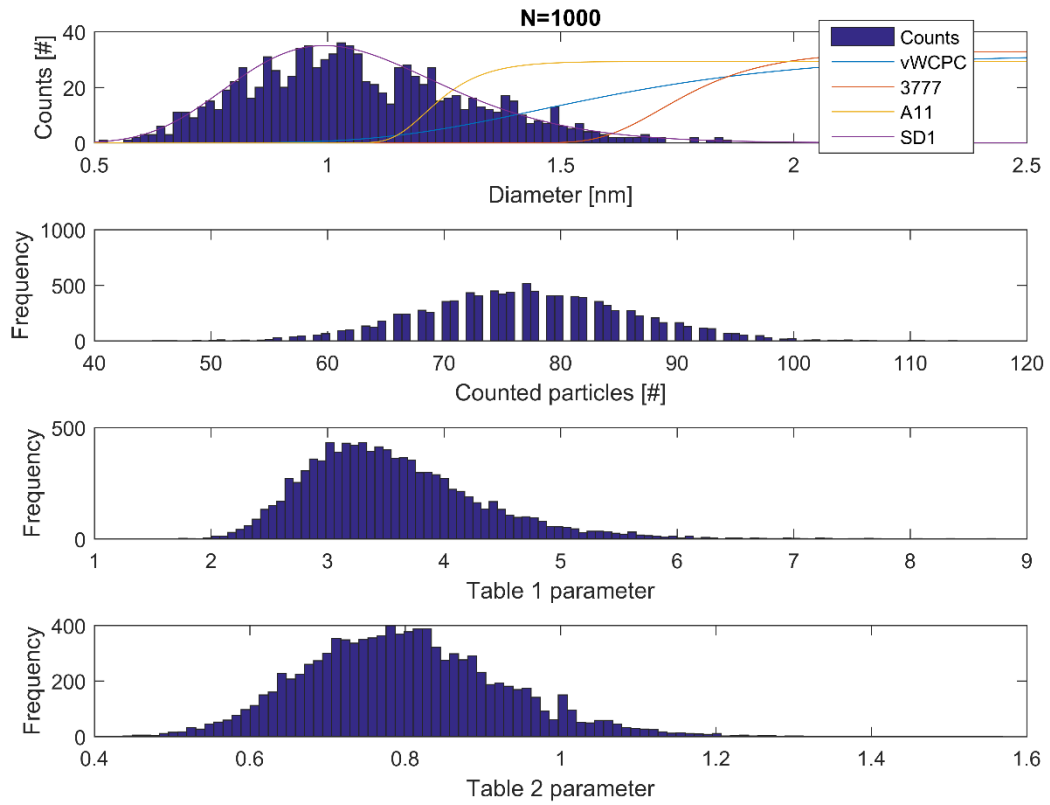

668

669   Figure 3. Counting statistics uncertainty for Poisson distribution. N is the number of counts.

670
671   Figure 4. PSM method calibration and transfer functions. Different colors represent different sizes (in
672   nm).
673

674
675 Figure 5. Upper panel: Example simulated distribution of SD1 with 1000 counts and on top plotted
676 CPC d50 curves. Second panel: counted particles by vWCPC in the 10000 simulations. Third panel:
677 Table 1 parameter for the vWCPC and SD1. Fourth panel: Table 2 parameter for the vWCPC and SD1.
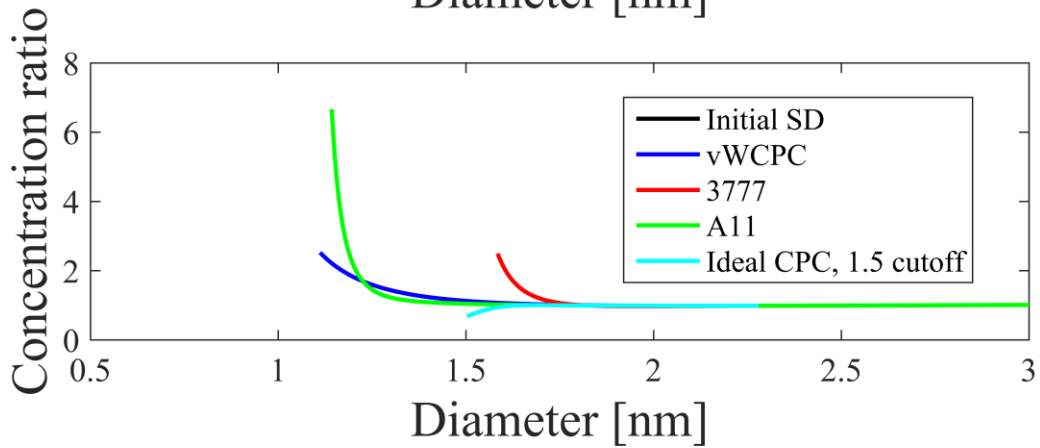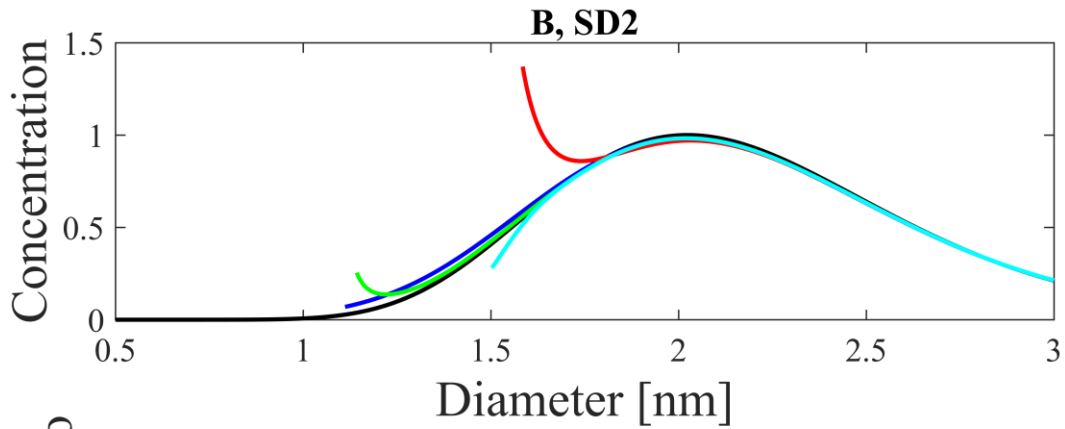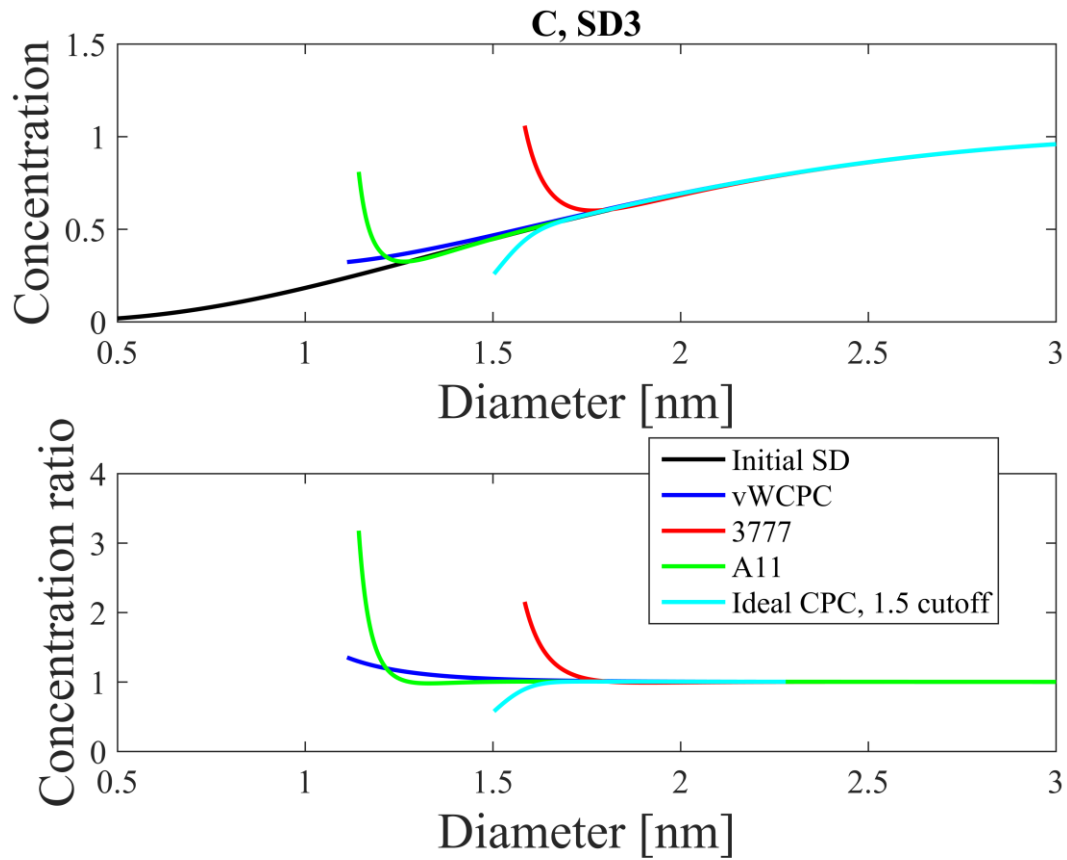678
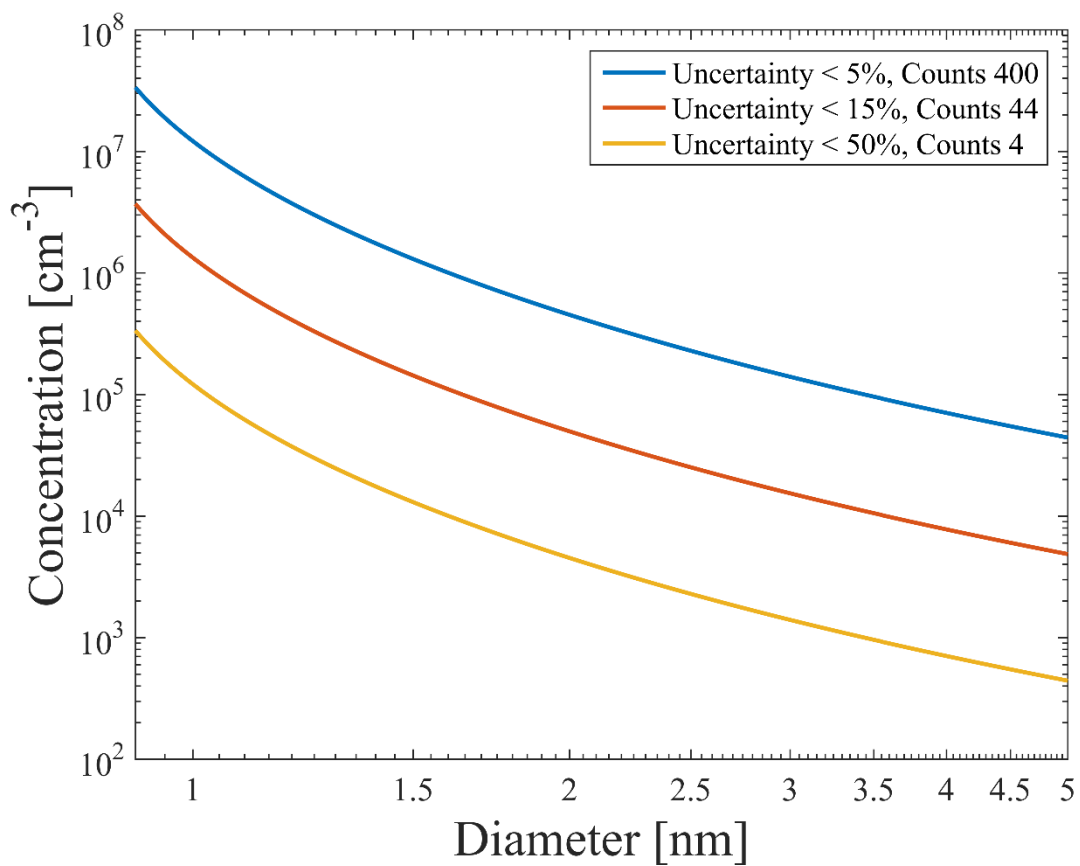
679
680 Figure 6. The DMA-CPC sampling an arbitrary particle size distribution. Lines show the particle
681 concentration required to reach statistical uncertainty smaller than 5%, 15% and 50% with the DMPS
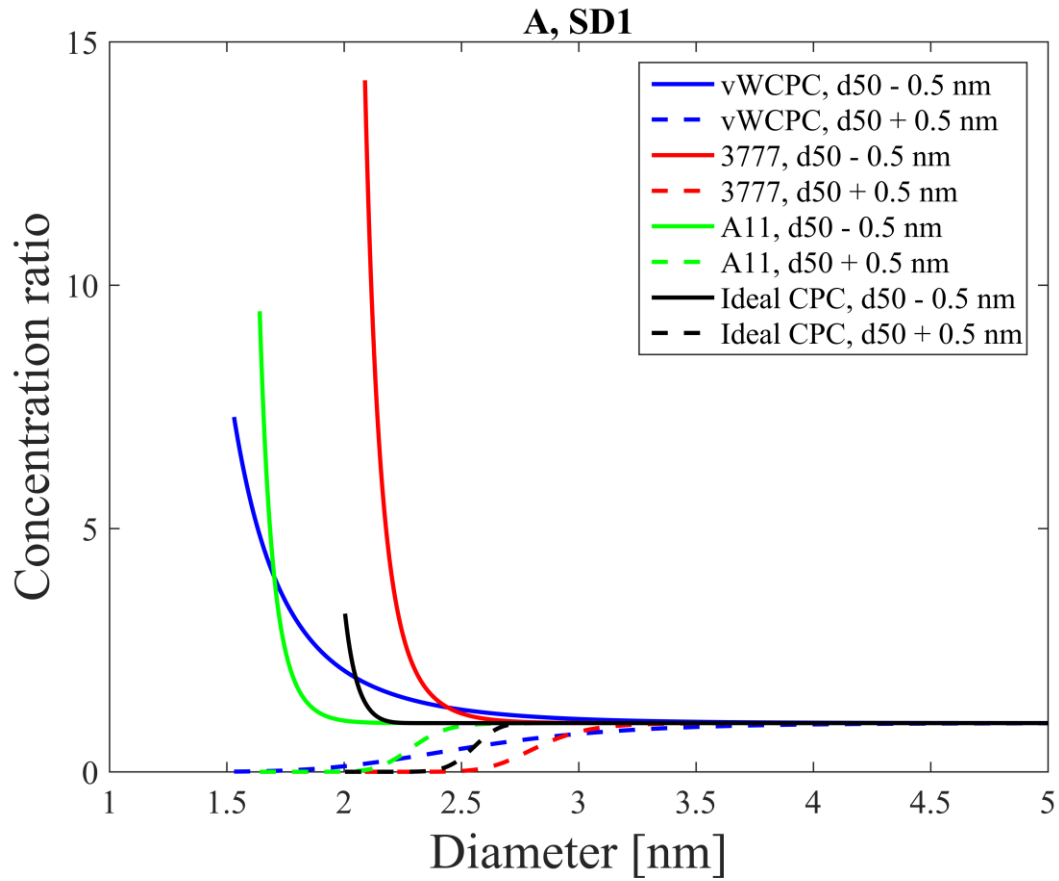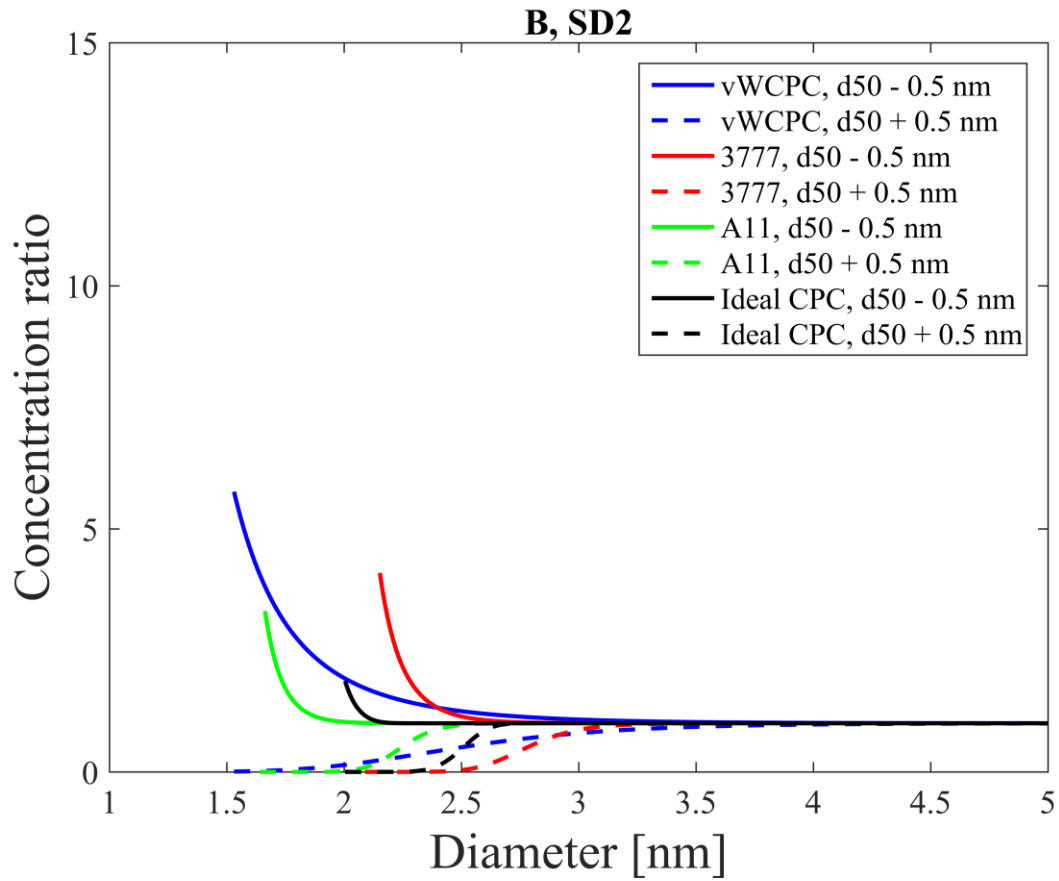682 published by Jiang et al. (2011b).
683

684

685
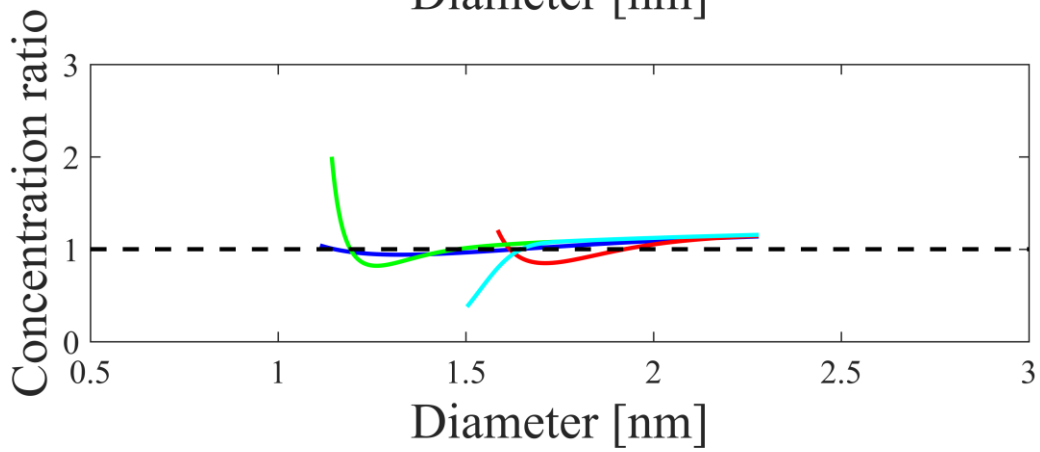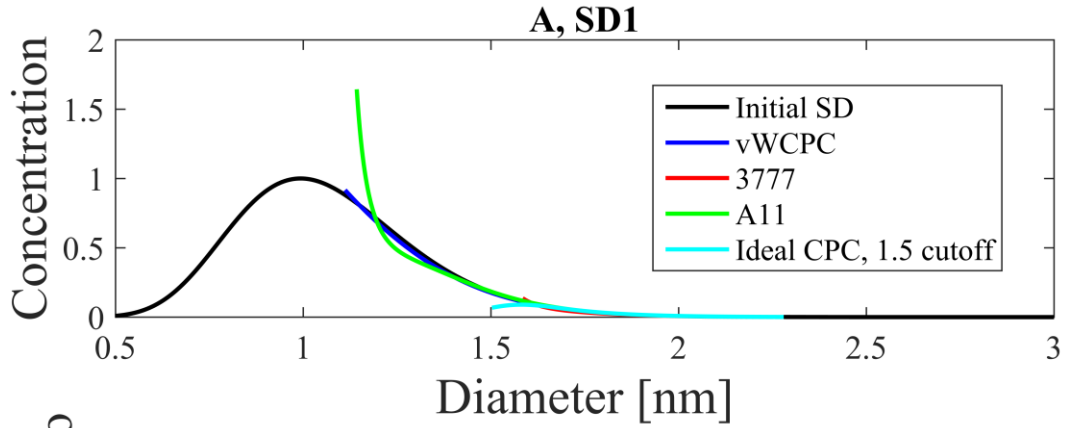
Figure 7. Inverted concentrations and the ratios of the inverted concentration to the initial size distributions for the case study 2, in which the size distributions were sampled with the DMA-CPC method. Note the different y-axis scales in lower panels.

A, SD1

Legend:
- vWCPC, d50 - 0.5 nm
- vWCPC, d50 + 0.5 nm
- 3777, d50 - 0.5 nm
- 3777, d50 + 0.5 nm
- A11, d50 - 0.5 nm
- A11, d50 + 0.5 nm
- Ideal CPC, d50 - 0.5 nm
- Ideal CPC, d50 + 0.5 nm

690

B, SD2

Legend:
- vWCPC, d50 - 0.5 nm
- vWCPC, d50 + 0.5 nm
- 3777, d50 - 0.5 nm
- 3777, d50 + 0.5 nm
- A11, d50 - 0.5 nm
- A11, d50 + 0.5 nm
- Ideal CPC, d50 - 0.5 nm
- Ideal CPC, d50 + 0.5 nm

691

Figure 8. The ratios of inverted concentration to initial size distribution for the case study 2 in which the size distributions were sampled with the DMA-CPC method. ±0.5 nm uncertainty is inserted to the d50 curve.

698
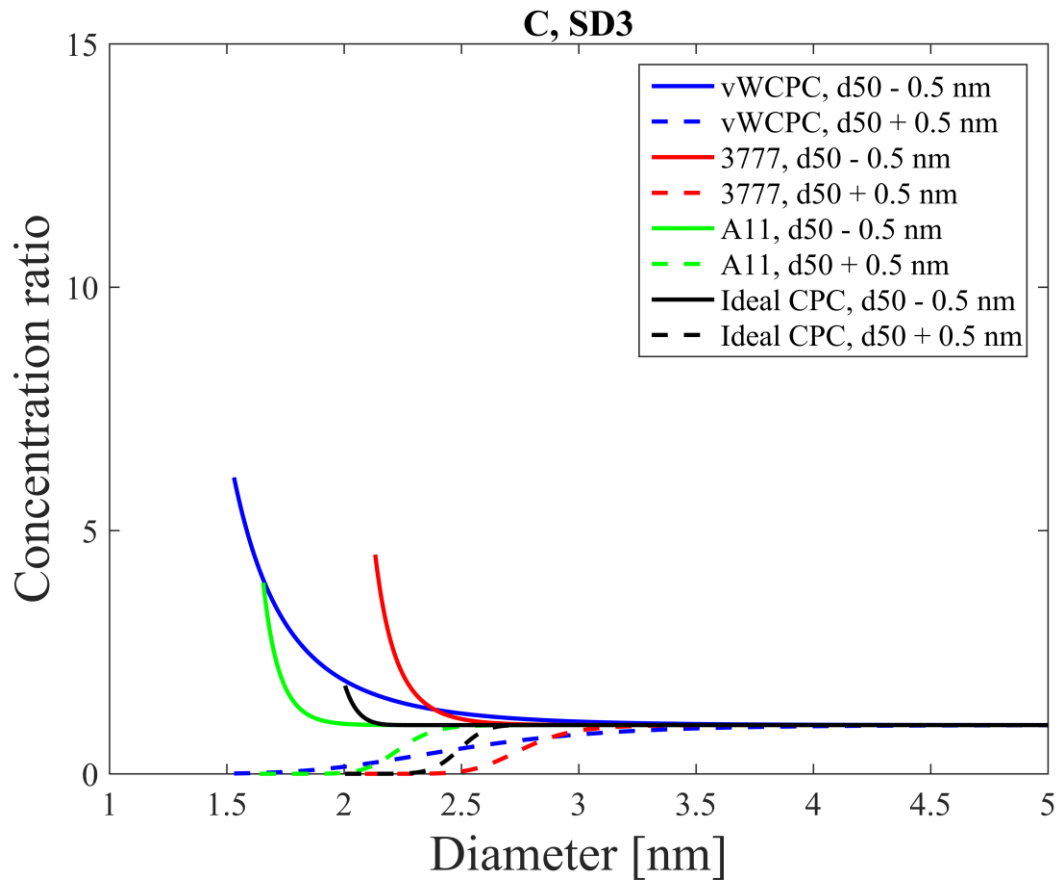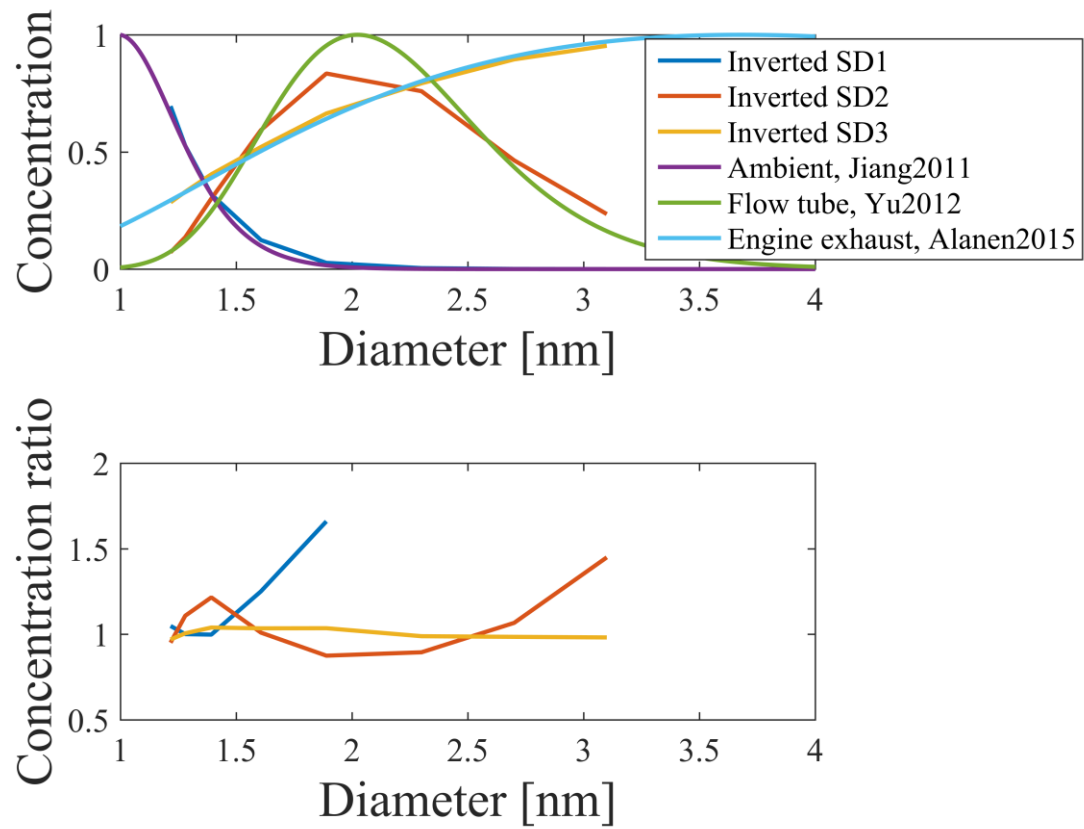699 Figure 9. Inverted concentrations and the ratios of the inverted concentration to the initial size
700 distributions in case study 4 with the PSM method.

A, SD1

Initial SD	
Inverted SD, d50 no error	
Inverted SD, d50 +0.5 nm error	
Inverted SD, d50 -0.5 nm error	
Inverted SD/Initial SD	
Inverted SD/Initial SD	
Inverted SD/Initial SD	

701

B, SD2

702
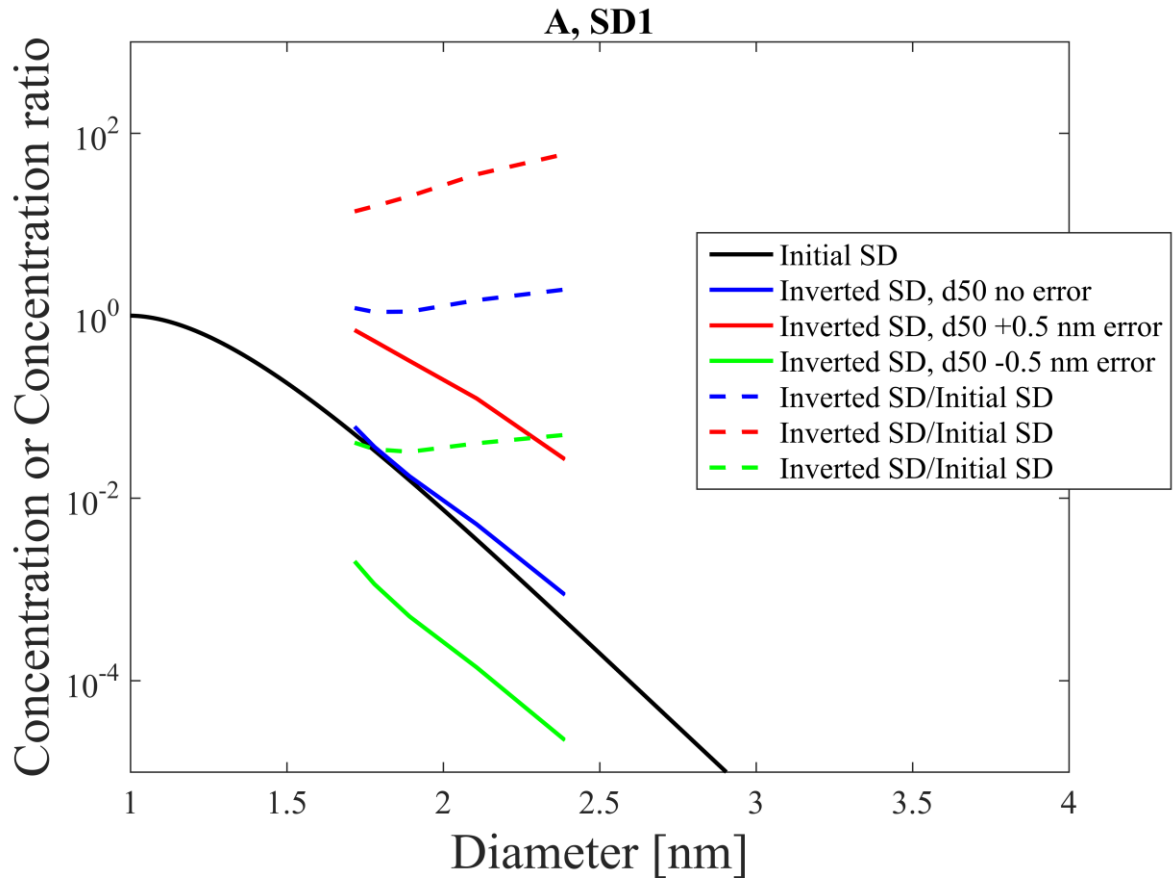
Figure 10. Inverted concentrations and the ratios for the case study 4.

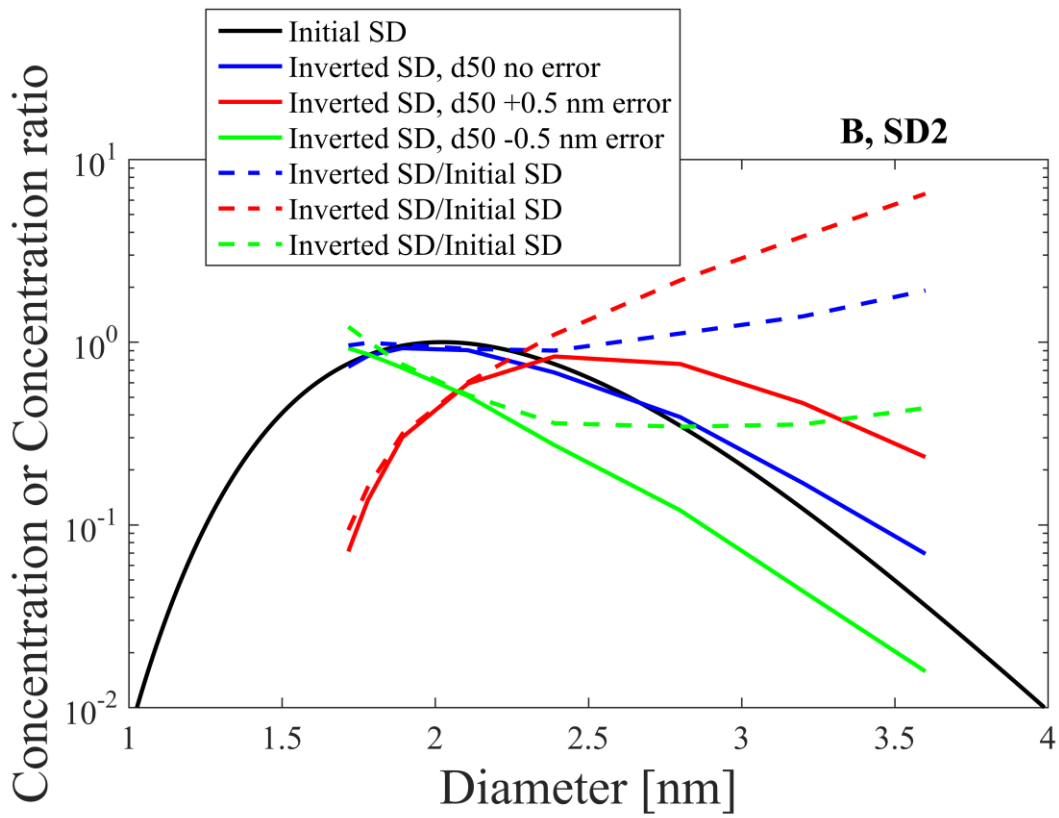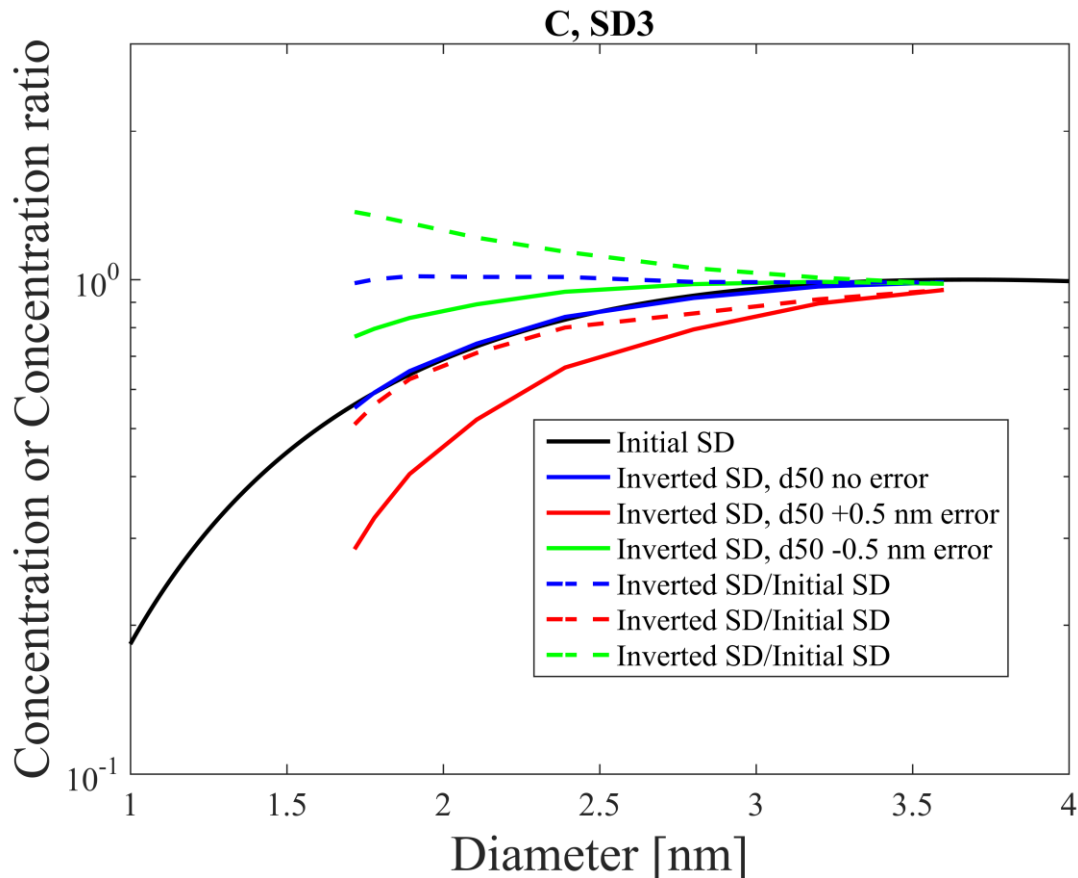Table 1. Statistical (std/mean, [%]) and Poisson (N/√N, [%]) uncertainties for the counted particles in the simulation of Figure 1.

$N_{detected,vWCPC}$	$Statistical_{vWCPC}$	$Poisson_{vWCPC}$	$N_{detected,3777}$	$Statistical_{3777}$	$Poisson_{3777}$	$N_{detected,A11}$	$Statistical_{A11}$	P
7.71	0.36	0.37	1.00	0.98	1.29	16.64	0.25	
77.05	0.11	0.11	9.73	0.32	0.32	166.18	0.08	
770.46	0.04	0.04	97.51	0.10	0.10	1663.40	0.02	
7698.70	0.01	0.01	973.26	0.03	0.03	16629.30	0.01	

Table 2. Statistical uncertainties (std/mean, [%]) for SD1 and each CPC for the parameter of Table 4 (Ratio of the detected concentration to the real concentration above the CPC d50 in Case 1)

vWCPC	3777	A11	$N_{sampled}$
NaN	1.41	0.18	1.00E+02
0.21	0.42	0.05	1.00E+03
0.06	0.10	0.02	1.00E+04
0.02	0.03	0.01	1.00E+05

Table 3. Statistical uncertainties (std/mean, [%]) for SD1 and each CPC for the parameter of Table 5 (Fraction of detected particles that are smaller than the nominal d50 of the CPCs for Case 1)

vWCPC	3777	A11	$N_{sampled}$
NaN	NaN	0.69	1.00E+02
0.16	0.64	0.21	1.00E+03

0.05	0.17	0.06	1.00E+04
0.02	0.05	0.02	1.00E+05

716

Table 4. Ratio of the detected concentration to the
real concentration above the CPC d50 in Case 1.

Instrument	SD1	SD2	SD3
vWCPC	3.72	0.88	0.98
3777	1.32	0.96	0.99
A11	1.00	0.99	1.00
Ideal CPC	1.00	1.00	1.00

717

718

Table 5. Fraction of detected particles that are
smaller than the nominal d50 of the CPCs for Case 1.

Instrument	SD1	SD2	SD3
vWCPC	0.67	0.04	0.02
3777	0.37	0.04	0.01
A11	0.12	0.00	0.00
Ideal CPC	0.00	0.00	0.00

719

Table 6a. Ratio of detected concentration to the real
concentration above the d50 with 0.5 nm error in d50
in Case 1

Instrument	SD1	SD2	SD3
vWCPC	0.03	0.40	0.87
3777	0.02	0.27	0.87
A11	0.02	0.43	0.88
Ideal CPC	0.02	0.33	0.88

720

Table 6b. Ratio of detected concentration to the real
concentration above the d50 with - 0.5 nm error in
d50 in Case 1

Instrument	SD1	SD2	SD3
vWCPC	14.25	1.69	1.12
3777	42.00	2.32	1.13
A11	24.75	1.33	1.10
Ideal CPC	37.59	1.75	1.12

721

722

723 **References**

724 Alanen, J., Saukko, E., Lehtoranta, K., Murtonen, T., Timonen, H., Hillamo, R., Karjalainen, P.,
725 Kuuluvainen, H., Harra, J., Keskinen, J., and Rönkkö, T.: The formation and physical properties of the
726 particle emissions from a natural gas engine, Fuel, 162, 155-161, 2015.

727

728 Almeida, J., Schobesberger, S., Kurten, A., Ortega, I. K., Kupiainen-Määttä, O., Praplan, A. P., Adamov,
729 A., Amorim, A., Bianchi, F., Breitenlechner, M., David, A., Dommen, J., Donahue, N. M., Downard, A.,

Dunne, E., Duplissy, J., Ehrhart, S., Flagan, R. C., Franchin, A., Guida, R., Hakala, J., Hansel, A., Heinritzi, M., Henschel, H., Jokinen, T., Junninen, H., Kajos, M., Kangasluoma, J., Keskinen, H., Kupc, A., Kurten, T., Kvashin, A. N., Laaksonen, A., Lehtipalo, K., Leiminger, M., Leppä, J., Loukonen, V., Makhmutov, V., Mathot, S., McGrath, M. J., Nieminen, T., Olenius, T., Onnela, A., Petäjä, T., Riccobono, F., Riipinen, I., Rissanen, M., Rondo, L., Ruuskanen, T., Santos, F. D., Sarnela, N., Schallhart, S., Schnitzhofer, R., Seinfeld, J. H., Simon, M., Sipilä, M., Stozhkov, Y., Stratmann, F., Tome, A., Tröstl, J., Tsagkogeorgas, G., Vaattovaara, P., Viisanen, Y., Virtanen, A., Vrtala, A., Wagner, P. E., Weingartner, E., Wex, H., Williamson, C., Wimmer, D., Ye, P. L., Yli-Juuti, T., Carslaw, K. S., Kulmala, M., Curtius, J., Baltensperger, U., Worsnop, D. R., Vehkamäki, H., and Kirkby, J.: Molecular understanding of sulphuric acid-amine particle nucleation in the atmosphere, Nature, 502, 359-363, 2013.

Alonso, M., Kousaka, Y., Nomura, T., Hashimoto, N., and Hashimoto, T.: Bipolar charging and neutralization of nanometer-sized aerosol particles, J Aerosol Sci, 28, 1479-1490, 1997.

Bertsekas, D. and Tsitsiklis, J.: Introduction to probability, Athena Scientific, 2002. 309-319, 2002.

Bianchi, F., Tröstl, J., Junninen, H., Frege, C., Henne, S., Hoyle, C. R., Molteni, U., Herrmann, E., Adamov, A., Bukowiecki, N., Chen, X., Duplissy, J., Gysel, M., Hutterli, M., Kangasluoma, J., Kontkanen, J., Kurten, A., Manninen, H. E., Munch, S., Perakylä, O., Petäjä, T., Rondo, L., Williamson, C., Weingartner, E., Curtius, J., Worsnop, D. R., Kulmala, M., Dommen, J., and Baltensperger, U.: New particle formation in the free troposphere: A question of chemistry and timing, Science, 352, 1109-1112, 2016.

Carbone, F., Attoui, M., and Gomez, A.: Challenges of measuring nascent soot in flames as evidenced by high-resolution differential mobility analysis, Aerosol Sci Tech, 50, 740-757, 2016.

Chen, D. R., Pui, D. Y. H., Hummes, D., Fissan, H., Quant, F. R., and Sem, G. J.: Design and evaluation of a nanometer aerosol differential mobility analyzer (Nano-DMA), J Aerosol Sci, 29, 497-509, 1998.

Ehn, M., Thornton, J. A., Kleist, E., Sipilä, M., Junninen, H., Pullinen, I., Springer, M., Rubach, F., Tillmann, R., Lee, B., Lopez-Hilfiker, F., Andres, S., Acir, I. H., Rissanen, M., Jokinen, T., Schobesberger, S., Kangasluoma, J., Kontkanen, J., Nieminen, T., Kurten, T., Nielsen, L. B., Jorgensen, S., Kjaergaard, H. G., Canagaratna, M., Maso, M. D., Berndt, T., Petäjä, T., Wahner, A., Kerminen, V. M., Kulmala, M., Worsnop, D. R., Wildt, J., and Mentel, T. F.: A large source of low-volatility secondary organic aerosol, Nature, 506, 476-479, 2014.

Eisele, F. L. and Tanner, D. J.: Measurement of the Gas-Phase Concentration of H2so4 and Methane Sulfonic-Acid and Estimates of H2so4 Production and Loss in the Atmosphere, J Geophys Res-Atmos, 98, 9001-9010, 1993.

Ezell, M. J., Chen, H., Arquero, K. D., and Finlayson-Pitts, B. J.: Aerosol fast flow reactor for laboratory studies of new particle formation, J Aerosol Sci, 78, 30-40, 2014.

Flagan, R. C.: On differential mobility analyzer resolution, Aerosol Sci Tech, 30, 556-570, 1999.

776   Fletcher, N. H.: Size Effect in Heterogeneous Nucleation, J Chem Phys, 29, 572-576, 1958.

777

778   Gamero-Castano, M. and Fernández de la Mora, J.: A condensation nucleus counter (CNC) sensitive
779   to singly charged sub-nanometer particles, J Aerosol Sci, 31, 757-772, 2000.

780

781   Hering, S. V., Stolzenburg, M. R., Quant, F. R., Oberreit, D. R., and Keady, P. B.: A laminar-flow, water-
782   based condensation particle counter (WCPC), Aerosol Sci Tech, 39, 659-672, 2005.

783

784   Hering, S. V., Lewis, G. L., Spielman, S. R., Eiguren-Fernandez, A., Kreisberg, N. M., Kuang, C., and
785   Attoui, M.: Detection near 1-nm with a Laminar-Flow, Water-Based Condensation Particle Counter,
786   Aerosol Sci Tech, 2016. 2016.

787

788   Hewitt, G. W.: The charging of small particles for electrostatic precipitation, American Institute of
789   Electrical Engineers Transactions, 76, 300-306, 1957.

790

791   Iida, K., Stolzenburg, M. R., and McMurry, P. H.: Effect of Working Fluid on Sub-2 nm Particle
792   Detection with a Laminar Flow Ultrafine Condensation Particle Counter, Aerosol Sci Tech, 43, 81-96,
793   2009.

794

795   Jiang, J. K., Attoui, M., Heim, M., Brunelli, N. A., McMurry, P. H., Kasper, G., Flagan, R. C., Giapis, K.,
796   and Mouret, G.: Transfer Functions and Penetrations of Five Differential Mobility Analyzers for Sub-2
797   nm Particle Classification, Aerosol Sci Tech, 45, 480-492, 2011a.

798

799   Jiang, J. K., Chen, M. D., Kuang, C. A., Attoui, M., and McMurry, P. H.: Electrical Mobility
800   Spectrometer Using a Diethylene Glycol Condensation Particle Counter for Measurement of Aerosol
801   Size Distributions Down to 1 nm, Aerosol Sci Tech, 45, 510-521, 2011b.

802

803   Jiang, J. K., Zhao, J., Chen, M. D., Eisele, F. L., Scheckman, J., Williams, B. J., Kuang, C. A., and
804   McMurry, P. H.: First Measurements of Neutral Atmospheric Cluster and 1-2 nm Particle Number
805   Size Distributions During Nucleation Events, Aerosol Sci Tech, 45, Ii-V, 2011c.

806

807   Jokinen, T., Sipilä, M., Junninen, H., Ehn, M., Lönn, G., Hakala, J., Petäjä, T., Mauldin, R. L., Kulmala,
808   M., and Worsnop, D. R.: Atmospheric sulphuric acid and neutral cluster measurements using CI-APi-
809   TOF, Atmos Chem Phys, 12, 4117-4125, 2012.

810

811   Kangasluoma, J., Kuang, C., Wimmer, D., Rissanen, M. P., Lehtipalo, K., Ehn, M., Worsnop, D. R.,
812   Wang, J., Kulmala, M., and Petäjä, T.: Sub-3 nm particle size and composition dependent response of
813   a nano-CPC battery, Atmos Meas Tech, 7, 689-700, 2014.

814

815   Kangasluoma, J., Attoui, M., Junninen, H., Lehtipalo, K., Samodurov, A., Korhonen, F., Sarnela, N.,
816   Schmidt-Ott, A., Worsnop, D., Kulmala, M., and Petäjä, T.: Sizing of neutral sub 3 nm tungsten oxide
817   clusters using Airmodus Particle Size Magnifier, J Aerosol Sci, 87, 53-62, 2015.

818

819   Kangasluoma, J., Franchin, A., Duplissy, J., Ahonen, L., Korhonen, F., Attoui, M., Mikkilä, J., Lehtipalo,
820   K., Vanhanen, J., Kulmala, M., and Petäjä, T.: Operation of the Airmodus A11 nano Condensation
821   Nucleus Counter at various inlet pressures, various operation temperatures and design of a new inlet
822   system, Atmos Meas Tech, 9, 2977-2988, 2016a.

823

824   Kangasluoma, J., Samodurov, A., Attoui, M., Franchin, A., Junninen, H., Korhonen, F., Kurtén, T.,
825   Vehkamäki, H., Sipilä, M., Lehtipalo, K., Worsnop, D., Petäjä, T., and Kulmala, M.: Heterogeneous
826   nucleation onto ions and neutralized ions - insights into sign-preference, Journal of Physical
827   Chemistry C, 120, 7444-7450, 2016b.

828

829   Kangasluoma, J., Hering, S., Picard, D., Lewis, G., Enroth, J., Korhonen, F., Kulmala, M., Sellegri, K.,
830   Attoui, M., and Petäjä, T.: Characterization of three new condensation particle counters for sub 3 nm
831   particle detection: ADI versatile water CPC, TSI 3777 nano enhancer and boosted 3010, Atmos Meas
832   Tech, Accepted, 2017.

833

834   Kirkby, J., Curtius, J., Almeida, J., Dunne, E., Duplissy, J., Ehrhart, S., Franchin, A., Gagne, S., Ickes, L.,
835   Kurten, A., Kupc, A., Metzger, A., Riccobono, F., Rondo, L., Schobesberger, S., Tsagkogeorgas, G.,
836   Wimmer, D., Amorim, A., Bianchi, F., Breitenlechner, M., David, A., Dommen, J., Downard, A., Ehn,
837   M., Flagan, R. C., Haider, S., Hansel, A., Hauser, D., Jud, W., Junninen, H., Kreissl, F., Kvashin, A.,
838   Laaksonen, A., Lehtipalo, K., Lima, J., Lovejoy, E. R., Makhmutov, V., Mathot, S., Mikkilä, J.,
839   Minginette, P., Mogo, S., Nieminen, T., Onnela, A., Pereira, P., Petäjä, T., Schnitzhofer, R., Seinfeld, J.
840   H., Sipilä, M., Stozhkov, Y., Stratmann, F., Tome, A., Vanhanen, J., Viisanen, Y., Vrtala, A., Wagner, P.
841   E., Walther, H., Weingartner, E., Wex, H., Winkler, P. M., Carslaw, K. S., Worsnop, D. R.,
842   Baltensperger, U., and Kulmala, M.: Role of sulphuric acid, ammonia and galactic cosmic rays in
843   atmospheric aerosol nucleation, Nature, 476, 429-433, 2011.

844

845   Kirkby, J., Duplissy, J., Sengupta, K., Frege, C., Gordon, H., Williamson, C., Heinritzi, M., Simon, M.,
846   Yan, C., Almeida, J., Tröstl, J., Nieminen, T., Ortega, I. K., Wagner, R., Adamov, A., Amorim, A.,
847   Bernhammer, A. K., Bianchi, F., Breitenlechner, M., Brilke, S., Chen, X. M., Craven, J., Dias, A.,
848   Ehrhart, S., Flagan, R. C., Franchin, A., Fuchs, C., Guida, R., Hakala, J., Hoyle, C. R., Jokinen, T.,
849   Junninen, H., Kangasluoma, J., Kim, J., Krapf, M., Kurten, A., Laaksonen, A., Lehtipalo, K.,
850   Makhmutov, V., Mathot, S., Molteni, U., Onnela, A., Perakylä, O., Piel, F., Petäjä, T., Praplan, A. P.,
851   Pringle, K., Rap, A., Richards, N. A. D., Riipinen, I., Rissanen, M. P., Rondo, L., Sarnela, N.,
852   Schobesberger, S., Scott, C. E., Seinfeld, J. H., Sipilä, M., Steiner, G., Stozhkov, Y., Stratmann, F.,
853   Tome, A., Virtanen, A., Vogel, A. L., Wagner, A. C., Wagner, P. E., Weingartner, E., Wimmer, D.,
854   Winkler, P. M., Ye, P. L., Zhang, X., Hansel, A., Dommen, J., Donahue, N. M., Worsnop, D. R.,
855   Baltensperger, U., Kulmala, M., Carslaw, K. S., and Curtius, J.: Ion-induced nucleation of pure
856   biogenic particles, Nature, 533, 521-526, 2016.

857

858   Knutson, E. and Whitby, K.: Aerosol classification by electric mobility: apparatus, theory, and
859   applications, J Aerosol Sci, 6, 443-451, 1975.

860

861   Kontkanen, J., Järvinen, E., Manninen, H., Lehtipalo, K., Kangasluoma, J., Decesari, S., Gobbi, G. P.,
862   Laaksonen, A., Petäjä, T., and Kulmala, M.: High concentrations of sub-3nm clusters and frequent
863   new particle formation observed in the Po Valley, Italy, during the PEGASOS 2012 campaign, Atmos
864   Chem Phys, 16, 1919-1935, 2016.

865

866 Kontkanen, J., Lehtipalo, K., Ahonen, L., Kangasluoma, J., Manninen, H. E., Hakala, J., Rose, C.,
867 Sellegri, K., Xiao, S., Wang, L., Qi, X., Nie, W., Ding, A., Yu, H., Lee, S., Kerminen, V. M., Petäjä, T., and
868 Kulmala, M.: Measurements of sub-3 nm particles using Particle Size Magnifier in different
869 environments: from clean mountain top to polluted megacities, Atmos Chem Phys, 17, 2163-2187,
870 2017.

871
872 Kuang, C., Chen, M., Zhao, J., Smith, J., McMurry, P. H., and Wang, J.: Size and time-resolved growth
873 rate measurements of 1 to 5 nm freshly formed atmospheric nuclei, Atmos Chem Phys, 12, 3573-
874 3589, 2012.

875
876 Kulmala, M., Petäjä, T., Nieminen, T., Sipilä, M., Manninen, H. E., Lehtipalo, K., Dal Maso, M., Aalto,
877 P. P., Junninen, H., Paasonen, P., Riipinen, I., Lehtinen, K. E. J., Laaksonen, A., and Kerminen, V. M.:
878 Measurement of the nucleation of atmospheric aerosol particles, Nat Protoc, 7, 1651-1667, 2012.

879
880 Kulmala, M., Kontkanen, J., Junninen, H., Lehtipalo, K., Manninen, H. E., Nieminen, T., Petäjä, T.,
881 Sipilä, M., Schobesberger, S., Rantala, P., Franchin, A., Jokinen, T., Järvinen, E., Äijalä, M.,
882 Kangasluoma, J., Hakala, J., Aalto, P. P., Paasonen, P., Mikkilä, J., Vanhanen, J., Aalto, J., Hakola, H.,
883 Makkonen, U., Ruuskanen, T., Mauldin, R. L., Duplissy, J., Vehkamäki, H., Bäck, J., Kortelainen, A.,
884 Riipinen, I., Kurten, T., Johnston, M. V., Smith, J. N., Ehn, M., Mentel, T. F., Lehtinen, K. E. J.,
885 Laaksonen, A., Kerminen, V. M., and Worsnop, D. R.: Direct Observations of Atmospheric Aerosol
886 Nucleation, Science, 339, 943-946, 2013.

887
888 Kulmala, M., Petäjä, T., Ehn, M., Thornton, J., Sipilä, M., Worsnop, D. R., and Kerminen, V. M.:
889 Chemistry of Atmospheric Nucleation: On the Recent Advances on Precursor Characterization and
890 Atmospheric Cluster Composition in Connection with Atmospheric New Particle Formation, Annu
891 Rev Phys Chem, 65, 21-37, 2014.

892
893 Lehtipalo, K., Leppä, J., Kontkanen, J., Kangasluoma, J., Franchin, A., Wimnner, D., Schobesberger, S.,
894 Junninen, H., Petäjä, T., Sipilä, M., Mikkilä, J., Vanhanen, J., Worsnop, D. R., and Kulmala, M.:
895 Methods for determining particle size distribution and growth rates between 1 and 3 nm using the
896 Particle Size Magnifier, Boreal Environ Res, 19, 215-236, 2014.

897
898 Lehtipalo, K., Rondo, L., Kontkanen, J., Schobesberger, S., Jokinen, T., Sarnela, N., Kurten, A., Ehrhart,
899 S., Franchin, A., Nieminen, T., Riccobono, F., Sipila, M., Yli-Juuti, T., Duplissy, J., Adamov, A., Ahlm, L.,
900 Almeida, J., Amorim, A., Bianchi, F., Breitenlechner, M., Dommen, J., Downard, A. J., Dunne, E. M.,
901 Flagan, R. C., Guida, R., Hakala, J., Hansel, A., Jud, W., Kangasluoma, J., Kerminen, V. M., Keskinen,
902 H., Kim, J., Kirkby, J., Kupc, A., Kupiainen-Maatta, O., Laaksonen, A., Lawler, M. J., Leiminger, M.,
903 Mathot, S., Olenius, T., Ortega, I. K., Onnela, A., Petaja, T., Praplan, A., Rissanen, M. P., Ruuskanen,
904 T., Santos, F. D., Schallhart, S., Schnitzhofer, R., Simon, M., Smith, J. N., Trostl, J., Tsagkogeorgas, G.,
905 Tome, A., Vaattovaara, P., Vehkamaki, H., Vrtala, A. E., Wagner, P. E., Williamson, C., Wimmer, D.,
906 Winkler, P. M., Virtanen, A., Donahue, N. M., Carslaw, K. S., Baltensperger, U., Riipinen, I., Curtius, J.,
907 Worsnop, D. R., and Kulmala, M.: The effect of acid-base clustering and ions on the growth of
908 atmospheric nano-particles, Nat Commun, 7, 2016.

909
910 Lindinger, W., Hansel, A., and Jordan, A.: Proton-transfer-reaction mass spectrometry (PTR-MS): on-
911 line monitoring of volatile organic compounds at pptv levels, Chem Soc Rev, 27, 347-354, 1998.

912

913 Lopez-Hilfiker, F. D., Mohr, C., Ehn, M., Rubach, F., Kleist, E., Wildt, J., Mentel, T. F., Carrasquillo, A. J.,
914 Daumit, K. E., Hunter, J. F., Kroll, J. H., Worsnop, D. R., and Thornton, J. A.: Phase partitioning and
915 volatility of secondary organic aerosol components formed from alpha-pinene ozonolysis and OH
916 oxidation: the importance of accretion products and other low volatility compounds, Atmos Chem
917 Phys, 15, 7765-7776, 2015.

918
919 Nosko, O., Vanhanen, J., and Olofsson, U.: Emission of 1.3–10 nm airborne particles from brake
920 materials, Aerosol Sci Tech, 51, 91-96, 2016.

921
922 Okuyama, K., Kousaka, Y., and Motouchi, T.: Condensational Growth of Ultrafine Aerosol-Particles in
923 a New Particle-Size Magnifier, Aerosol Sci Tech, 3, 353-366, 1984.

924
925 Premnath, V., Oberreit, D., and Hogan, C. J.: Collision-Based Ionization: Bridging the Gap between
926 Chemical Ionization and Aerosol Particle Diffusion Charging, Aerosol Sci Tech, 45, 712-726, 2011.

927
928 Seto, T., Okuyama, K., de Juan, L., and Fernández de la Mora, J.: Condensation of supersaturated
929 vapors on monovalent and divalent ions on varying size, J Chem Phys, 107, 1576-1585, 1997.

930
931 Sipilä, M., Sarnela, N., Jokinen, T., Henschel, H., Junninen, H., Kontkanen, J., Richters, S.,
932 Kangasluoma, J., Franchin, A., Perakylä, O., Rissanen, M. P., Ehn, M., Vehkamaki, H., Kurten, T.,
933 Berndt, T., Petäjä, T., Worsnop, D., Ceburnis, D., Kerminen, V. M., Kulmala, M., and O'Dowd, C.:
934 Molecular-scale evidence of aerosol particle formation via sequential addition of HIO3, Nature, 537,
935 532-534, 2016.

936
937 Smith, J. N., Barsanti, K. C., Friedli, H. R., Ehn, M., Kulmala, M., Collins, D. R., Scheckman, J. H.,
938 Williams, B. J., and McMurry, P. H.: Observations of aminium salts in atmospheric nanoparticles and
939 possible climatic implications, P Natl Acad Sci USA, 107, 6634-6639, 2010.

940
941 Stolzenburg, M. R. and McMurry, P. H.: An Ultrafine Aerosol Condensation Nucleus Counter, Aerosol
942 Sci Tech, 14, 48-65, 1991.

943
944 Stolzenburg, M. R. and McMurry, P. H.: Equations governing single and tandem DMA configurations
945 and a new lognormal approximation to the transfer function, Aerosol Sci Tech, 42, 421-432, 2008.

946
947 Tröstl, J., Chuang, W. K., Gordon, H., Heinritzi, M., Yan, C., Molteni, U., Ahlm, L., Frege, C., Bianchi, F.,
948 Wagner, R., Simon, M., Lehtipalo, K., Williamson, C., Craven, J. S., Duplissy, J., Adamov, A., Almeida,
949 J., Bernhammer, A. K., Breitenlechner, M., Brilke, S., Dias, A., Ehrhart, S., Flagan, R. C., Franchin, A.,
950 Fuchs, C., Guida, R., Gysel, M., Hansel, A., Hoyle, C. R., Jokinen, T., Junninen, H., Kangasluoma, J.,
951 Keskinen, H., Kim, J., Krapf, M., Kurten, A., Laaksonen, A., Lawler, M., Leiminger, M., Mathot, S.,
952 Mohler, O., Nieminen, T., Onnela, A., Petäjä, T., Piel, F. M., Miettinen, P., Rissanen, M. P., Rondo, L.,
953 Sarnela, N., Schobesberger, S., Sengupta, K., Sipilä, M., Smith, J. N., Steiner, G., Tome, A., Virtanen,
954 A., Wagner, A. C., Weingartner, E., Wimmer, D., Winkler, P. M., Ye, P. L., Carslaw, K. S., Curtius, J.,
955 Dommen, J., Kirkby, J., Kulmala, M., Riipinen, I., Worsnop, D. R., Donahue, N. M., and Baltensperger,
956 U.: The role of low-volatility organic compounds in initial particle growth in the atmosphere, Nature,
957 533, 527-531, 2016.

958

959 Vanhanen, J., Mikkilä, J., Lehtipalo, K., Sipilä, M., Manninen, H. E., Siivola, E., Petäjä, T., and Kulmala,
960 M.: Particle Size Magnifier for Nano-CN Detection, Aerosol Sci Tech, 45, 533-542, 2011.

961
962 Wang, Y., Kangasluoma, J., Attoui, M., Fang, J., Junninen, H., Kulmala, M., Petäjä, T., and Biswas, P.:
963 Observation of incipient particle formation during flame synthesis by tandem differential mobility
964 analysis-mass spectrometry (DMA-MS), Proceedings of the Combustion Institute (in press), 2016. 1-
965 8, 2016.

966
967 Wang, Y., Kangasluoma, J., Attoui, M., Fang, J., Junninen, H., Kulmala, M., Petäjä, T., and Biswas, P.:
968 The high charge fraction of flame-generated particles in the size range below 3 nm measured by
969 enhanced particle detectors, Combust Flame, 176, 72-80, 2017.

970
971 Wiedensohler, A. and Fissan, H. J.: Bipolar Ion and Electron-Diffusion Charging of Aerosol-Particles in
972 High-Purity Argon and Nitrogen, Particle & Particle Systems Characterization, 7, 250-255, 1990.

973
974 Wiedensohler, A., Birmili, W., Nowak, A., Sonntag, A., Weinhold, K., Merkel, M., Wehner, B., Tuch, T.,
975 Pfeifer, S., Fiebig, M., Fjaraa, A. M., Asmi, E., Sellegri, K., Depuy, R., Venzac, H., Villani, P., Laj, P.,
976 Aalto, P., Ogren, J. A., Swietlicki, E., Williams, P., Roldin, P., Quincey, P., Huglin, C., Fierz-
977 Schmidhauser, R., Gysel, M., Weingartner, E., Riccobono, F., Santos, S., Gruning, C., Faloon, K.,
978 Beddows, D., Harrison, R. M., Monahan, C., Jennings, S. G., O'Dowd, C. D., Marinoni, A., Horn, H. G.,
979 Keck, L., Jiang, J., Scheckman, J., McMurry, P. H., Deng, Z., Zhao, C. S., Moerman, M., Henzing, B., de
980 Leeuw, G., Loschau, G., and Bastian, S.: Mobility particle size spectrometers: harmonization of
981 technical standards and data structure to facilitate high quality long-term observations of
982 atmospheric particle number size distributions, Atmos Meas Tech, 5, 657-685, 2012.

983
984 Wimmer, D., Lehtipalo, K., Franchin, A., Kangasluoma, J., Kreissl, F., Kurten, A., Kupc, A., Metzger, A.,
985 Mikkilä, J., Petäjä, T., Riccobono, F., Vanhanen, J., Kulmala, M., and Curtius, J.: Performance of
986 diethylene glycol-based particle counters in the sub-3 nm size range, Atmos Meas Tech, 6, 1793-
987 1804, 2013.

988
989 Winkler, P. M., Steiner, G., Vrtala, A., Vehkamäki, H., Noppel, M., Lehtinen, K. E. J., Reischl, G. P.,
990 Wagner, P. E., and Kulmala, M.: Heterogeneous nucleation experiments bridging the scale from
991 molecular ion clusters to nanoparticles, Science, 319, 1374-1377, 2008.

992
993 Yu, H., McGraw, R., and Lee, S. H.: Effects of amines on formation of sub-3 nm particles and their
994 subsequent growth, Geophys Res Lett, 39, 2012.

995
996 Yu, H., Gannet Hallar, A., You, Y., Sedlacek, A., Springston, S., Kanawade, V., Lee, Y. N., Wang, J.,
997 Kuang, C., McGraw, R. L., McCubbin, I., Mikkilä, J., and Lee, S. H.: Sub-3 nm particles observed at the
998 coastal and continental sites in the United States, Journal of Geophysical Research: Atmospheres,
999 119, 860-879, 2014.

1000
1001